



## Review article

## BODIPY in Alzheimer's disease diagnostics: A review



Daniil Abramchuk<sup>a,b</sup>, Alevtina Voskresenskaya<sup>a</sup>, Ilia Kuzmichev<sup>c</sup>, Alexander Erofeev<sup>a,b</sup>, Peter Gorelkin<sup>a,b</sup>, Maxim Abakumov<sup>b,d</sup>, Elena Beloglazkina<sup>a</sup>, Olga Krasnovskaya<sup>a,b,\*</sup>

<sup>a</sup> Chemistry Department, Lomonosov Moscow State University, Leninskie gory 1,3, 119991, Moscow, Russia

<sup>b</sup> Department of Materials Science of Semiconductors and Dielectrics, National University of Science and Technology (MISIS), Leninsky prospect 4, 101000, Moscow, Russia

<sup>c</sup> V.P. Serbsky National Medical Research Center for Psychiatry and Narcology, Kropotkinsky per. 23, 119034, Moscow, Russia

<sup>d</sup> Department of Medical Nanobiotechnology, N.I. Pirogov Russian National Research Medical University, Ostrovityanova str., 1, 6, 117997, Moscow, Russia

## ARTICLE INFO

## Keywords:

BODIPY  
Alzheimer's disease  
Diagnostics  
Optical visualization  
Fluorescent probes  
Amyloid plaques  
Neurofibrillary tangles

## ABSTRACT

Timely diagnosis and therapy of Alzheimer's disease remains one of the greatest questions in medicinal chemistry of neurodegenerative disease. The lack of low-cost sensors capable of reliable detection of structural changes in AD-related proteins is the driving factor for the development of novel molecules with affinity for AD hallmarks. The development of cheap, safe diagnostic methods is a highly sought-after area of research. Optical fluorescent probes are of great interest due to their non-radioactivity, low cost, and ability of the real-time visualization of AD hallmarks. Boron dipyrromethene (BODIPY)-based fluorophore is one promising fluorescent unit for *in vivo* labeling due to its high photostability, easy modification, low toxicity, and cell-permeability. In recent years, many fluorescent BODIPY-based probes capable of A $\beta$  plaque, A $\beta$  soluble oligomers, neurofibrillary tangles (NFT) optical detection, as well as probes with copper ion chelating units and viscosity sensors have been developed. In this review, we summarized BODIPY derivatives as fluorescent sensors capable of detecting pathological features of Alzheimer's disease, published from 2009 to 2023, as well as their design strategies, optical properties, and *in vitro* and *in vivo* activities.

## 1. Introduction

Alzheimer's disease (AD) is a complex neurodegenerative disorder, that is characterized by such cognitive disfunctions as memory loss, speech and writing disturbance, depression, disorder of logical thinking, etc. Over 50 million people are living with AD or dementia, and this number is predicted to grow to 152-million-cases level by 2050 [1]. Due to the absence of effective therapy, early-stage diagnosis of AD is strongly desired [2]. Pathological features of AD are extracellular neurotic plaque composed of misfolded amyloid-beta (A $\beta$ ) peptides and intracellular neurofibrillary tangles (NFT) composed of hyperphosphorylated tau proteins [3]. A $\beta$  exists in a dynamic equilibrium among various monomeric, oligomeric, and higher-order filamentous forms that differ in synaptotoxic properties [4]. Soluble A $\beta$  oligomers are the most neurotoxic form of misfolded A $\beta$  and affect intracellular viscosity [5,6]. Another pathogenic factor of AD is metal dyshomeostasis, which results in the copper ions accumulation and the formation of A $\beta$ -Cu aggregates [7].

Since A $\beta$  is widely recognized as a primary neuropathologic agent in AD, diverse diagnostic techniques, such as single photon emission computed tomography (SPECT), positron emission tomography (PET), and magnetic resonance imaging (MRI), have been used for A $\beta$  mapping [8,9]. We recently summarized the use of metal-based drugs for MRI, SPECT, and PET visualization of amyloid plaques [10,11]. However, the application of these probes still has several risks. The use of MRI requires large doses of drugs to obtain high-resolution images, and what is more important, the MRI technique can only detect A $\beta$  plaques larger than 50  $\mu$ m, while the size of A $\beta$  plaques is usually in the range of 20–60  $\mu$ m [12]. As for PET and SPECT techniques, the use of radioactive isotopes imposes several restrictions; their high cost and radioactivity limit their practical application. Therefore, optical imaging offers real-time, high-resolution imaging, leading to rapid, inexpensive, and nonradioactive visualization of AD-caused deposits [13]. Thus, the design, synthesis, and investigation of fluorescent probes for imaging the pathological signatures of Alzheimer's disease have already become the subject of several reviews [14–17].

\* Corresponding author. Chemistry Department, Lomonosov Moscow State University, Leninskie gory 1,3, 119991 Moscow, Russia.

E-mail address: [krasnovskayao@gmail.com](mailto:krasnovskayao@gmail.com) (O. Krasnovskaya).

<https://doi.org/10.1016/j.ejmech.2024.116682>

Received 18 June 2024; Received in revised form 11 July 2024; Accepted 12 July 2024

Available online 20 July 2024

0223-5234/© 2024 Elsevier Masson SAS. All rights are reserved, including those for text and data mining, AI training, and similar technologies.

In the past two decades, mounting interest in the development of optical probes for AD diagnosis led to avalanche number of fluorescent markers for AD species detection. Thus, numerous derivatives generally based on curcumin, coumarin, boron dipyrromethene (BODIPY) and cyanine structures were designed. Several fluorescent probes, such as IRI-1, CRANAD-3, DANIR-3b-c, AOI-987 etc. demonstrated the capability of A $\beta$  and NFTs visualization *in vivo* (Fig. 1) [18]. However, none of the fluorescent probes have been approved for clinical use yet due to the significant background interference and poor tissue penetration of the required excitation beam [19].

Boron dipyrromethene (BODIPY) fluorophores are one of the most promising fluorescent units for biolabeling purposes, with high photostability, fluorescence quantum yields, easy modification options, robustness against chemicals, and excitation/emission wavelengths in the visible spectral region [20,21]. Moreover, BODIPY derivatives recently demonstrated the ability to inhibit acetylcholinesterase (AChE) which is interest in development of BODIPY-based theranostics agents for AD treatment [22]. Since 2009, when the first fluorescent BODIPY-based probe for NFT detection was reported by Ojida et al. [23], a large number of BODIPY-based fluorescent sensors for the detection of different AD hallmarks have been reported. BODIPY-based fluorescent probes capable of NFTs [23–27] and A $\beta$  plaque [28–33] detection, as well as probes with copper ion chelating units [34] and viscosity sensors [6,35] were developed, and the ability for A $\beta$  and NFTs visualization *in vivo* was demonstrated [24,32,33,36]. However, only one review reported by Dzyuba summarized the use of BODIPY as an imaging agent for A $\beta$ -related processes [37]. Herein, we summarize the application of BODIPY-based fluorescent probes for different AD hallmarks's detection and briefly discuss the physical aspect of the design of fluorescent probes.

## 2. BODIPY-based probes for A $\beta$ and soluble oligomer detection: summary

The design of fluorescent probes for the detection of pathological hallmarks of AD is a challenging task. So that the fluorescent probe would be able to detect the AD hallmark *in vivo*, it should have a suitable oil–water partition coefficient ( $2 < \log P < 5$ ) and molecular weight (MW < 500 Da) to guarantee satisfactory BBB penetration [32,33]. Also, maxima of emission and excitation of probes are strongly desired to be arranged in the NIR region ( $\lambda > 700$  nm) due to the high tissue penetration ability of near-infrared light [38]. Also, the probe should have high selectivity and affinity for the AD hallmark [39]. Herein, we summarized photophysical properties ( $\lambda_{ex}$ ,  $\lambda_{em}$ ,  $\lambda_{abs}$ , fluorescence quantum yield), A $\beta$  affinity data, molar masses, brain uptake/washout rates, results of *in vivo* imaging, and the difference in fluorescent signals between AD and WT mice published between 2009 and 2023 (Table 1) [6,23–36,40–47].

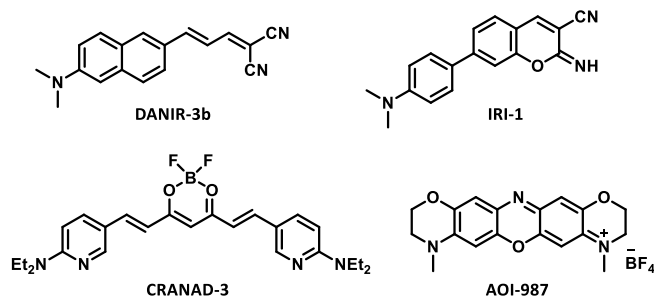


Fig. 1. Fluorescent probes IRI-1, CRANAD-3, DANIR-3b and AOI-987 for *in vivo* A $\beta$  detection [18].

## 3. Fluorescent probes: design

The concept of a fluorescent probe implies that the molecule will either not fluoresce before binding to the target or will significantly change its emissive properties after binding to it. A decrease in the fluorescence of a probe is usually achieved by either photoinduced electron transfer (PIET), intramolecular electron transfer (ICT), or twisted intramolecular electron transfer (TICT). Each of these effects leads to a significant probe's fluorescence quenching in non-bound form; target binding leads to conformational restrictions and ICT or PIET disturbance, which results in significant fluorescence enhancement. Since these two physical phenomena play a critical role in fluorescent probe design, we discuss each of these effects below [48–55].

### 3.1. Twisted intramolecular charge transfer (TICT)

Intramolecular charge transfer (ICT) is a fundamental mechanism that plays essential roles in materials science, biology, and medicine [48]. ICT-based probes are usually based on the electron push-pull substituent effect when charge redistribution occurs from the electron donor to the acceptor system [49]. The electron density in the fluorophore is strongly affected by the donor group, and coordination between the target and donor groups results in significant changes in fluorescence emission [50].

One of the subtypes of ICT is twisted ICT (TICT), which is implemented in molecular rotors that consist of two fragments that can rotate relative to each other, a stator and a rotor. Upon excitation, molecular rotors undergo a transformation into a twisted state as a result of charge transfer and the subsequent rotation of molecule parts relative to each other. Such conformational transitions lead to the conversion of absorbed energy into thermal motion, which results in the radiation-free relaxation of excited probe molecules and a decrease in their quantum yields [50]. When a TICT-based probe binds to protein or enters a viscous environment, free-rotation hindrance results in fluorescence enhancement (Fig. 2) [51,52]. The most prominent example of a TICT-probe is a Thioflavin-T (ThT) with a rotatable single bond between N,N-dimethylaniline and thiazole quaternary ammonium salt, which is a gold standard probe for A $\beta$  visualization [53]. However, the application of ThT *in vivo* has been hindered because of restricted BBB penetration and a short emission wavelength [54].

### 3.2. Photoinduced electron transfer (PIET)

Photoinduced electron transfer (PIET) is another commonly used mechanism in the design of fluorescent probes [40,55]. Since PIET efficiency is less sensitive to surrounding polarities, this mechanism is more desirable for the development of fluorescent probes to stain biomolecules. A PIET-based fluorescent probe is commonly designed as a fluorophore conjugated with an electron-rich ligand, which quenches its fluorescence. Upon energy absorption, a fluorophore enters the excited state, followed by electron transfer from the HOMO of the electron-donor ligand to the single-occupied HOMO of the fluorophore unit. This transfer prevents the reverse electron transition from LUMO to HOMO of the fluorophore fragment, resulting in decreased molecule fluorescence [55]. When a PIET-based fluorescent probe binds to a protein target, emerging conformational restrictions prevent electron transfer from an electron-donor ligand, which results in fluorescence enhancement (Fig. 2). Thus, the quenching efficiency of the PIET mechanism is governed by the oxidation potential of the PIET donor, the distance between the donor and the fluorophore, and the energy gap between the HOMOs of a fluorophore and an electron donor [40,55]. PIET-based fluorescent probes are also of great interest for the development of diagnostic agents for AD due to their higher sensitivity and fluorescence turn-on selectivity compared to ICT-based analogues [40].

**Table 1**Photophysical properties and A $\beta$  affinity data of BODIPY derivatives 1–75 and *in vivo* tests data, molar masses, and lipophilicity of BODIPY-based probes 1, 13, 15, 17, 20, 45, 64, 67, 71 and 73.

Probe		K <sub>d</sub> , nM	$\lambda_{\text{ex}}$ , nm	$\lambda_{\text{em}}$ , nm	$\lambda_{\text{abs}}$ , nm	$\phi$ , %	Solvent	Reference
<b>BODIPY-based probes for A<math>\beta</math> detection</b>								
<b>ICT-based probes</b>								
1	[125I] BODIPY7	108	No data	613	606	36	No data	[28]
2	BAP-1	44.1	614	648	604	46.8	CHCl <sub>3</sub>	[29]
3	BAP-2	54.6 $\pm$ 7.0	650	708	651	11.4	CHCl <sub>3</sub>	[30]
4	BAP-3	149 $\pm$ 15	663	705	665	4.5	CHCl <sub>3</sub>	
5	BAP-4	26.8 $\pm$ 2.8	636	704	623	9.3	CHCl <sub>3</sub>	
6	BAP-5	18.1 $\pm$ 1.3	649	723	639	4.3	CHCl <sub>3</sub>	
7	EUA-1	322.8 $\pm$ 119.5	No data	654	518	12	CHCl <sub>3</sub>	[31]
8	EUA-2	226.2 $\pm$ 127.1	No data	667	597	7	CHCl <sub>3</sub>	
9	EUA-3	320.1 $\pm$ 161.1	No data	736	677	1	CHCl <sub>3</sub>	
10	EUA-4	48.6 $\pm$ 9.7	No data	673	624	13	CHCl <sub>3</sub>	
11	EUA-5	96.9 $\pm$ 41.9	No data	763	721	3	CHCl <sub>3</sub>	
12	TPyrBDP	54.2 $\pm$ 5.8	No data	752	675	No data	DMSO	[32]
13	TPipBDP	28.3 $\pm$ 5.9	No data	751	653	No data	DMSO	
14	THAIBDP	28.2 $\pm$ 3.1	No data	758	676	No data	DMSO	
15	BocBDP	67.8 $\pm$ 3.2	578	588	No data	No data	DCM	[33]
<b>PIET-based probes</b>								
16a	Probe1	3.5	485	505	497	No data	EtOH	[40]
17	QAD-1	6	No data	755	645	No data	DMSO	[36]
<b>BODIPY-based probes with copper chelator units</b>								
18	BDA	No data	460	503	No data	No data	No data	[34]
<b>Viscosity sensitive BODIPY-based fluorescent probes</b>								
19	BODIPY-1	No data	No data	No data	No data	No data	No data	[6]
20	5-MB-SZ	155.8	No data	552	505	34.0	DCM	[35]
21	B-SZ	177.4	No data	551	512	13.3	DCM	
22	BD-SZ	No data	No data	578	532	18.0	DCM	
<b>BODIPY-based probes for soluble oligomers detection</b>								
23	1	No data	512	525	No data	No data	No data	[41]
24	2	No data	525	538	No data	No data	No data	
25	5	No data	No data	530	520	3	Water	
26	6	No data	No data	542	529	1	Water	
27	1	No data	No data	672	650	34	CHCl <sub>3</sub>	[42,43]
28	BD-Oligo	480	No data	604	580	8.7	DMSO	[44]
29	NB	6.4	688	753	No data	No data	CHCl <sub>3</sub>	[45]
30	BAOP-1	83.8 $\pm$ 67.8	610	657	610	55.0	CHCl <sub>3</sub>	[46]
31	BAOP-2	201 $\pm$ 27	619	671	616	30.0	CHCl <sub>3</sub>	
32	BAOP-3	108 $\pm$ 12	623	728	623	8.96	CHCl <sub>3</sub>	
33	BAOP-4	148 $\pm$ 18	604	663	603	47.8	CHCl <sub>3</sub>	
34	BAOP-5	50.6 $\pm$ 5.5	619	674	614	48.1	CHCl <sub>3</sub>	
35	BAOP-6	107 $\pm$ 13	593	679	593	37.8	CHCl <sub>3</sub>	
36	BAOP-7	54.7 $\pm$ 13.7	618	677	616	40.4	CHCl <sub>3</sub>	
37	BAOP-8	121 $\pm$ 34	599	674	596	44.3	CHCl <sub>3</sub>	
38	BAOP-9	No data	No data	No data	No data	No data	No data	
39	BAOP-10	62.4 $\pm$ 3.1	590	649	589	51.0	CHCl <sub>3</sub>	
40	BAOP-11	85.4 $\pm$ 5.1	593	677	591	44.3	CHCl <sub>3</sub>	
41	BAOP-12	297 $\pm$ 27	578	615	584	19.9	CHCl <sub>3</sub>	
42	BAOP-13	229 $\pm$ 27	593	666	591	23.0	CHCl <sub>3</sub>	
43	BAOP-14	500 $\pm$ 93	580	624	579	33.7	CHCl <sub>3</sub>	
44	BAOP-15	90.8 $\pm$ 5.5	619	694	616	11.4	CHCl <sub>3</sub>	
45	BAOP-16	34.3 $\pm$ 4.0	635	704	638	22.0	CHCl <sub>3</sub>	
46	BAOP-17	74.4 $\pm$ 6.3	602	650	603	18.2	CHCl <sub>3</sub>	
<b>BODIPY-based probes for intraneuronal neurofibrillary tangles (NFTs) detection</b>								
47	1	9·10 <sup>3</sup>	No data	547	520	31	Water	[23]
48	2	No data	No data	No data	No data	No data	No data	
49	Tau-1	No data	No data	705	621	23.6	CHCl <sub>3</sub>	[24]
50	Tau-2	No data	No data	687	597	28.0	CHCl <sub>3</sub>	
51	BD-tau	No data	525	590	No data	3	Water	[25]
52	BDNCA318	No data	525	580	No data	4	Water	
53	5a	No data	No data	565	555	17.1	MeOH	[26]

(continued on next page)

Table 1 (continued)

Probe		$K_d$ , nM	$\lambda_{ex}$ , nm	$\lambda_{em}$ , nm	$\lambda_{abs}$ , nm	$\phi$ , %	Solvent	Reference
54	5b	No data	No data	574	561	18.2	MeOH	
55	5c	No data	No data	589	569	24.0	MeOH	
56	5d	No data	No data	562	552	35.5	MeOH	
57	5e	No data	No data	590	566	27.6	MeOH	
58	5f	No data	No data	629	590	17.0	MeOH	
59	5g	No data	No data	640	598	0.9	MeOH	
60	5h	No data	No data	680	599	1.3	MeOH	
61	5i	No data	No data	579	569	47.1	MeOH	
62	5j	No data	No data	635	595	13.7	MeOH	
63	TNIR7-0A	125.8 ± 42.4	550	740	520	No data	DMSO	[27]
64	TNIR7-1A	16.8 ± 2.3	592	774	570	No data	DMSO	
65	TNIR7-2A	13.7 ± 1.1	602	815	584	No data	DMSO	
66	TNIR7-0B	124.8 ± 29.5	510	656	505	No data	DMSO	
67	TNIR7-1B	12.7 ± 3.6	550	716	545	No data	DMSO	
68	TNIR7-2B	47.5 ± 2.9	565	776	557	No data	DMSO	
69	TNIR7-7	620 ± 177	572	724	528		DMSO	[47]
70	TNIR7-9	105 ± 26	598	774	578	12.2	DCM	
71	TNIR7-10	289 ± 121	600	771	584	52.8	DMSO	
72	TNIR7-8	>1000	535	711	531	50.7	DCM	
73	TNIR7-11	92.6 ± 27.8	560	716	549	10.0	DMSO	
74	TNIR-7-12	23.2 ± 5.9	604	816	595		DMSO	
75	TNIR7-13	11.8	No data	No data	No data	24.9	DCM	
						No data	No data	

**In vivo efficacy data**

Probe	Molar mass	Log P	BBB penetration rate, %ID/g	Fluorescence intensities ratio (time postinjection)	Washout rate (brain $N$ min/ $N$ min)
<b>A<math>\beta</math> detection</b>					
1	530.18	No data	0.40 (2 min)	No data	2.9 (2 min/60 min)
13	425.35	3.60	10.38 ± 4.11	4.2 (18 min)	No data
15	451.32	3.74	No data	3.6 (5 min)	No data
17	559.53	No data	9.11 (5 min)	1.5 (5 min)	10 (5 min/30 min)
<b>Viscosity detection</b>					
20	395.28	2.62	No data	2.2 (45 min)	No data
<b>Soluble oligomers detection</b>					
45	533.43	No data	0.428 (2 min)	1.5 (30 min)	6.4 (2 min/60 min)
<b>NFT detection</b>					
49	377.25	No data	No data	No data	No data
64	387.24	3.79	4.43 ± 0.29 (2 min)	1.13 (20 min)	3.3 (2 min/60 min)
67	388.23	3.38	8.57 ± 0.70 (2 min)	No data	6.2 (2 min/60 min)
70	417.27	No data	3.68 (2 min)	No data	4.2 (2 min/60 min)
73	418.25	No data	4.57 (2 min)	No data	10.9 (2 min/60 min)

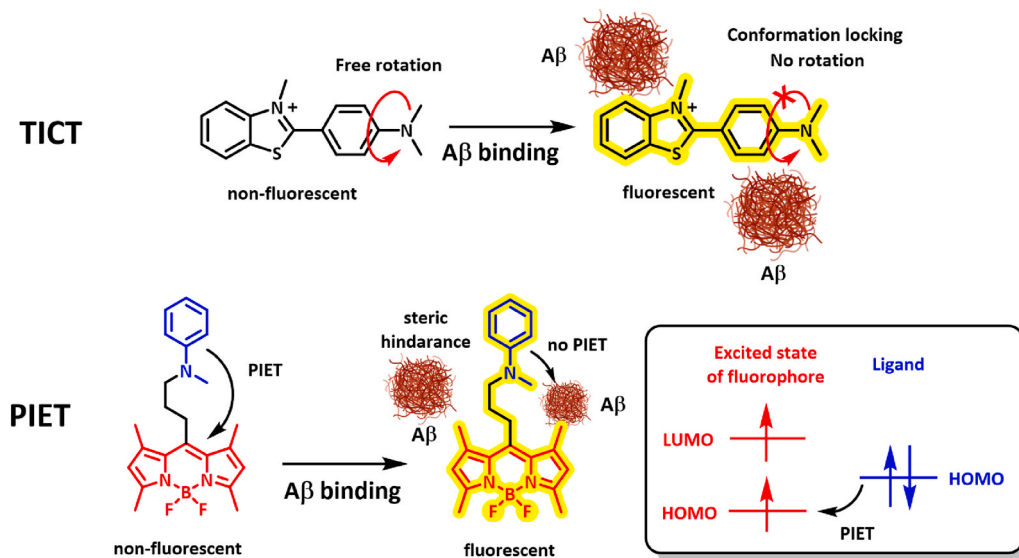


Fig. 2. Mechanisms of fluorescence quenching by TICT and PIET effects.

#### 4. BODIPY-based probes for A $\beta$ detection

##### 4.1. Probes for A $\beta$ detection with a TICT-based fluorescence quenching mechanism

Since optical imaging of A $\beta$  aggregates *in vivo* is a challenging task, different classes of fluorophores were proposed as drug candidates. «Push-pull» thiophen-based NIR NIAD-4 dye has previously shown high specificity for A $\beta$  plaque labeling *in vivo* [56]. In 2010, BODIPY-based fluorescent probe **1** with a NIAD-4 moiety in the structure for dual SPECT and fluorescence imaging was designed (Fig. 3) [28]. Despite probe **1** exhibiting high affinity to A $\beta$  aggregates and good co-localization with ThS in a fluorescence staining experiment on Tg2576 mouse brain sections, BODIPY [<sup>125</sup>I] **1** exhibited relatively low brain uptake *in vivo* (0.4 % ID/g at 2 min postinjection (p.i.). In 2012–2013, Saji et al. reported BODIPY-based probes **2–6** that were designed by modifying BODIPY **1** and its derivatives with terminal dimethyl amino rotor units [29,30] (Fig. 3). BODIPYs **2–6** exhibited high affinity for A $\beta$  aggregates and fluorescence enhancement in the presence of A $\beta$  species. Also, high probe **2–6** selectivity to A $\beta$  plaques in Tg2576 mouse brain sections was confirmed by a fluorescence staining experiment with ThS and A $\beta$  targeted BC05 antibodies. However, *in vivo* studies demonstrated scalp accumulation of BODIPY **2** and **3** both in Tg2576 and WT mice.

In an attempt to improve the pharmacokinetic properties of BODIPY **2** and **3**, Sozmen et al. designed five styryl-conjugated BODIPY-based probes **7–11** by varying the nature and position of styryl-conjugated moieties [31] (Fig. 4). BODIPY **10** displayed the highest A $\beta$  affinity in the saturation assay. However, *in vitro* assays demonstrated only particular co-localization of probes **7**, **8** and **10** with ThS on Tg2576 mouse brain slices.

Recently, in 2023, Ma et al. presented three well-designed probes **12–14** with a cyclic amine group as a rotor unit [32] (Fig. 5). Gaussian theoretical calculations revealed charge transfer from the HOMO of the styryl moiety to the LUMO of the electron deficient BODIPY core. Molecular docking performed with the 5KK3 model confirmed probes binding with A $\beta$  plaques by interaction with Lys16, Val18, and Glu22 amino acid residues. Probes **12–14** exhibited high selectivity for A $\beta$  binding in fluorescence staining experiments on brain slices of the hippocampus and cortex of APP/PS1 mice. Also, the biocompatibility of probes was confirmed to be appropriate for *in vivo* studies by the low cytotoxicity shown on PC12 cells and the low hemolysis rate. *In vivo* assays showed the ability of BODIPY **13** to penetrate the BBB and detect A $\beta$  plaques using a near-infrared fluorescence imaging system. The fluorescence signal intensities of APP/PS1 and WT mice differed by a 3-fold ratio.

Also, in 2023 Zhu et al. designed probe **15** with an NHBoc terminal group, which was intended as a donor of additional hydrogen bonds with Lys16, Val18, and Glu22 amino acid residues in A $\beta$  [33] (Fig. 6).

Docking studies conducted with the 5KK3 model confirmed the formation of hydrogen bonds between NHBoc and Lys16, Val18, and Glu22 amino acid residues, which may potentially reduce the washout rate of the probe. The presence of ICT in BODIPY **15** was confirmed by a Gaussian theoretical calculation. *In vivo* assays revealed the ability of BODIPY **15** for *in vivo* A $\beta$  aggregate detection via a 1.5-fold difference in fluorescence signals between the WT and APP/PS1 groups of mice. Also, conjugate **15** showed the ability to detect A $\beta$  plaques *in vivo* within 2 h, exceeding the detection time of A $\beta$  aggregates using other previously reported probes.

##### 4.2. Probes for A $\beta$ detection with a PIET-based fluorescence quenching mechanism

The development of probes based on PIET fluorescence quenching mechanism is more difficult than the design of classic “push-pull” donor-acceptor ICT-based probes. Only in 2015, Ren et al. reported the first BODIPY-based probe with a PIET-based fluorescence quenching mechanism. Probe **16a** was designed via conjugation of the PIET-donor aniline moiety onto the *meso*-position of the BODIPY core [40] (Fig. 7). Comparison of fluorescence intensities of probe **16a** and BODIPYs **16b–e** demonstrated that the PIET effect and fluorescence intensity decrease are more pronounced in less sterically hindered structures. Probe **16a** exhibited high affinity and selectivity for binding with A $\beta$  plaques. Moreover, BODIPY **16a** adversely affected a much lower level of side interactions in an *in vitro* fluorescent co-staining experiment on the unwashed cortex brain sections of APPsw/PS1De9 mice when compared with ICT-based ThT and CRANAD-58.

In 2018, the same group designed the PIET-based probe **17**, enhanced by TICT-based fluorescence quenching mechanisms via the dimethylaminothiophene unit [36] (Fig. 8). Theoretical molecular orbital level predictions performed by DFT and TDDFT showed that the energy level of HOMO in tetrahydro quinoxaline (−4.76 eV) is between HOMO and LUMO in the BODIPY unit (−5.90 eV and −2.15 eV, respectively), which makes this electron-donating group suitable for PIET from the quinoxaline unit to the BODIPY core. The quantum yield of **17**'s precursor without a tetrahydroquinoxaline moiety was ten times higher than that of probe **17**, thus proving a PIET fluorescence quenching mechanism in BODIPY **17**. Probe **17** demonstrated high affinity for A $\beta$  species and fluorescence enhancement in the presence of A $\beta$  aggregates. High colocalization between BODIPY **17**, ThS, and anti-A $\beta$  ab2454 antibodies proved high selectivity of probe binding. Biodistribution experiments demonstrated rapid brain uptake and washout of probe **17**. *In vivo* visualization by IVIS revealed an ability of **17** to detect A $\beta$  plaques in APP<sup>sw</sup>/PSEN1De9 mice, with a 1.5-fold difference in the fluorescence signal intensities of Tg and WT mice.

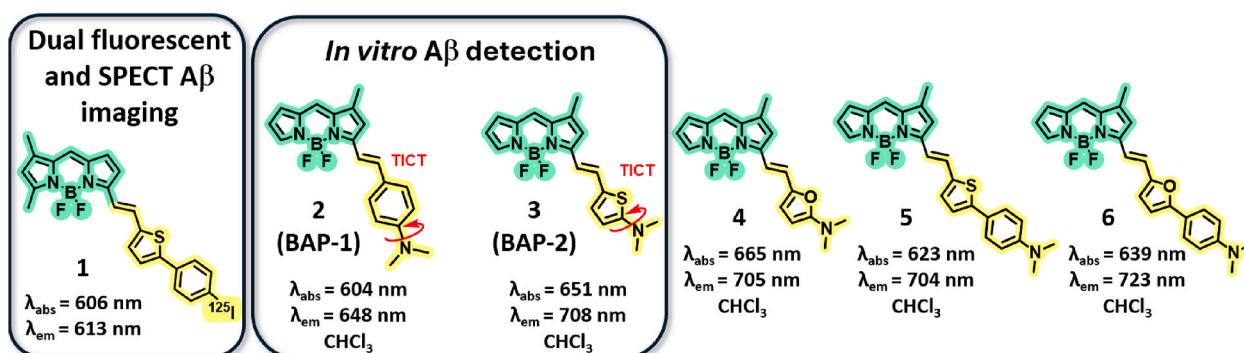


Fig. 3. BODIPY-based probe **1** for SPECT and fluorescence A $\beta$  plaques visualization, designed by Ono et al. [28] and BODIPY-based probes **2–6** for fluorescent detection of A $\beta$  plaques, reported by Saji et al. [29,30].

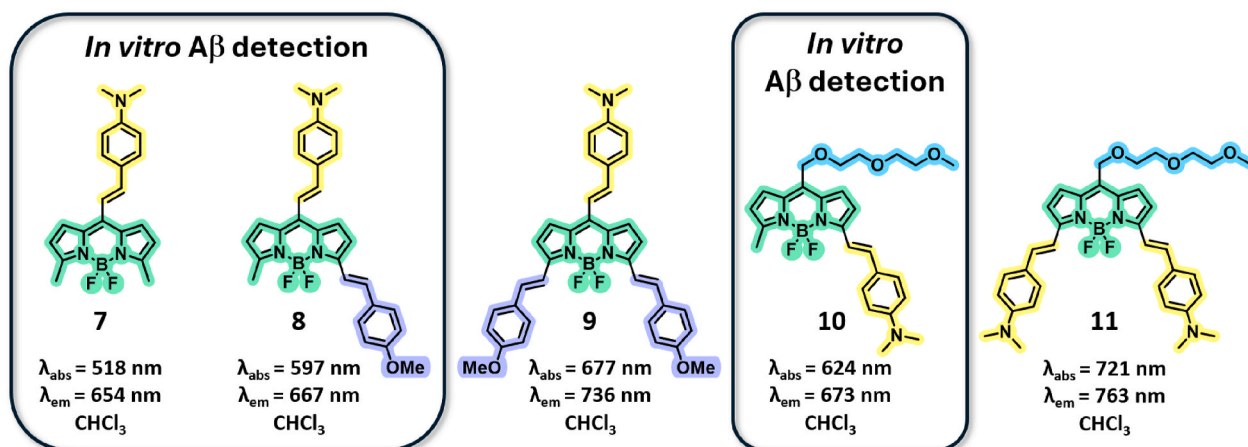


Fig. 4. BODIPY-based fluorescent probes 7–11 published by Sozmen et al. [31].

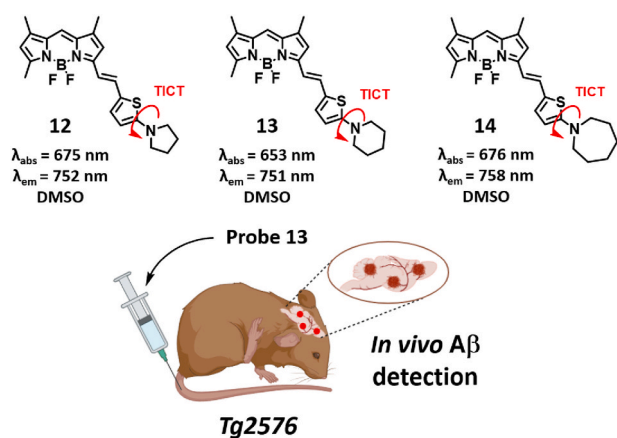


Fig. 5. TICT-based probes 12–14 for optical A $\beta$  detection reported by Ma et al. [32].

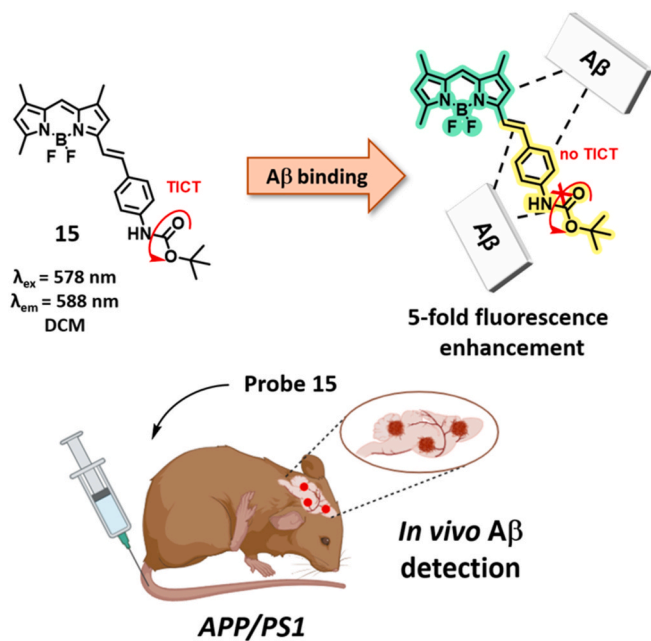


Fig. 6. Probe 15 for optical A $\beta$  detection published by Zhu et al. [33].

#### 4.3. BODIPY-based probes with copper chelator units

The role of copper cations in the pathology of Alzheimer's disease, as well as the therapeutic strategy of chelating metal cations, has been repeatedly discussed [7]. The development of fluorescent probes capable of chelating metal cations is promising, as it opens opportunities for the design of theranostic probes. In 2015, Kong et al. reported bifunctional BODIPY **18** both for binding with A $\beta$  aggregates and for chelating copper ions [34] (Fig. 9). Probe **18** fluorescence quenching while copper ion chelating was demonstrated by titration with  $\text{CuCl}_2$  solution. Also, TEM imaging revealed the ability of BODIPY **18** to inhibit Cu-induced A $\beta$  aggregation and the formation of A $\beta$ -Cu-**18** nanospheres. Nevertheless, Cu-**18** complexes demonstrated notable neurotoxicity in the MTT assay on SHSY-5Y cells.

#### 4.4. Viscosity-sensitive BODIPY-based fluorescent probes

Abnormal deviations in cellular viscosity are another pathological hallmark associated with AD. Thus, monitoring viscosity fluctuations can provide valuable insights into the pathogenesis and diagnosis of AD [57,58]. In 2018, Kubankova et al. reported probe **19** modified with an alkyl ammonium moiety, which showed the ability to accumulate in cell plasma membranes [6] (Fig. 10). BODIPY **19** demonstrated a linear dependence of fluorescence lifetime on medium viscosity in methanol-glycerol solutions. Moreover, probe **19** revealed the temperature-dependent changes in plasma membrane viscosity of SH-SY5Y cells. A $\beta_{1-42}$  aggregates destroy giant plasma membrane vesicles (GPMVs), the plasma membranes of HeLa and SH-SY5Y cells, which leads to a reduction in microviscosity and quenching of the **19**'s fluorescence; fibrillar A $\beta_{1-42}$  did not cause a significant effect. Also, the ability of the neuroprotective peptide H3 to counteract changes in microviscosity caused by A $\beta$  species has been proven by the absence of fluorescence quenching.

Another viscosity monitoring strategy for AD imaging was proposed by Wang et al. in 2022 [35]. Three BODIPY-based bifunctional fluorescent probes **20–22** for dual-functional imaging of A $\beta$  aggregates and intracellular viscosity change detection were reported (Fig. 11). Conjugates **20–22** were designed by coupling a fluorescent BODIPY core and a benzothiazole group as a molecular rotor. Probes **20** and **21** showed high selectivity for binding with A $\beta$  aggregates over BSA and HSA in PBS solution. *Ex vivo* assays on APP/PS1 mouse cortex brain slices showed high co-localization of BODIPYs **20** and **21** probes with ThS. The ability of BODIPYs **20** and **21** to determine cell viscosity changes was also confirmed by fluorescence enhancement during incubation with lipopolysaccharide or nystatin-pretreated SHSY-5Y cells. Further assays showed that probe **20** can be applied for A $\beta$  plaque *in vivo* detection due

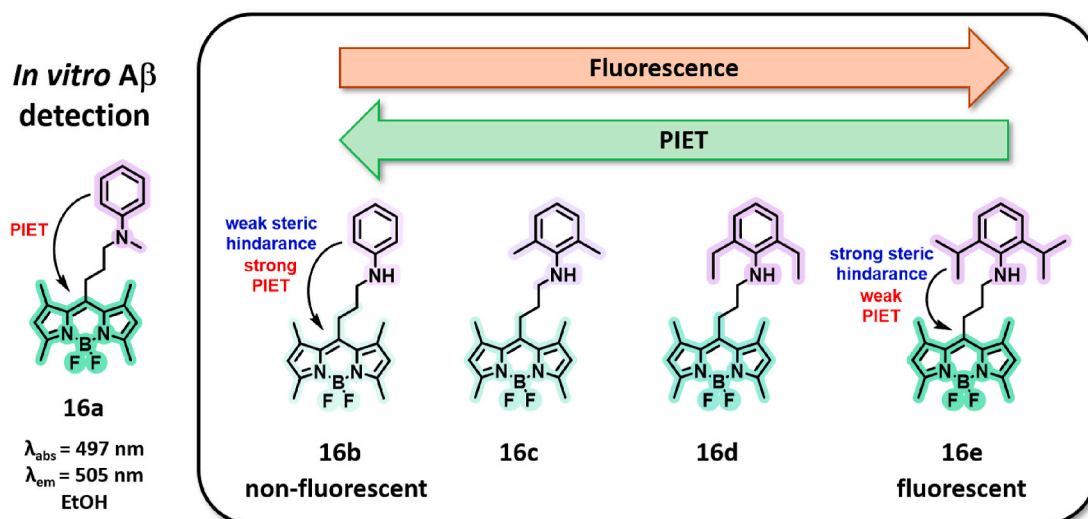


Fig. 7. BODIPY-based probe 16a with PIET fluorescence quenching mechanism and derivatives 16b-e, reported by Ren et al. [40].

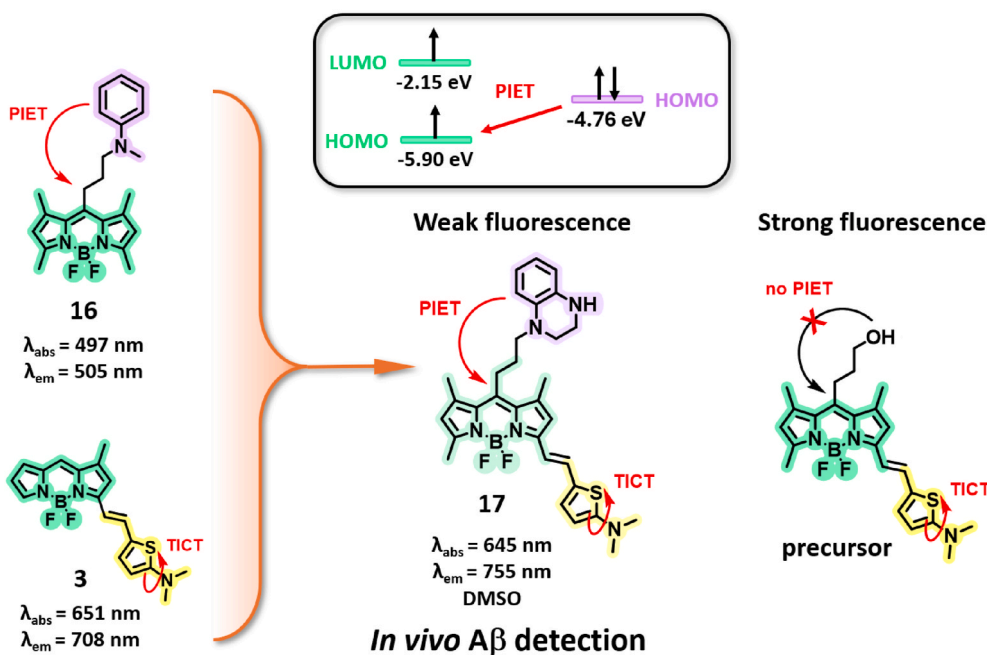


Fig. 8. BODIPY 17 with dual PIET and ICT fluorescence quenching mechanisms published by Ren et al. [36].

to the approximately 2-fold difference in fluorescence intensities among APP/PS1 and WT mice.

#### 4.5. BODIPY-based probes for soluble oligomer detection

As A $\beta$  oligomers exhibit the highest neurotoxicity among other A $\beta$  species, significant correlations between A $\beta$  soluble oligomer level and cognitive dysfunction were observed (Fig. 12) [59]. Soluble A $\beta$  oligomers directly bind to neurons with high affinity and block plasticity mechanisms related to learning and memory, trigger the loss of excitatory synapses, and eventually cause cell death [60]. Also, A $\beta$  oligomer formation refers to the early stages of AD, thus making it a promising target both for AD pre-symptomatic diagnosis and monitoring of patients' assessments [61]. A lot of evidence suggests that oligomers have a complex, highly organized, and heterogeneous structure. Thus, A $\beta$  oligomers, which consist of A $\beta$  dimers, trimers, hexamers, and dodecamers, as well as larger oligomers. The triangular A $\beta$  trimer model is

commonly fitted into a triangular cavity, and T- and V-shapes are considered promising molecular shapes to design A $\beta$  oligomer-targeting fluorescent probes [62,63].

BODIPY-based fluorescent probes capable of distinguishing one type of oligomer in the presence of another were first proposed in 2010 by Smith et al. [41]. Thus, four BODIPY-based probes 23–26 for ordered A $\beta$  oligomer recognition in the presence of unordered ones were designed (Fig. 13). All probes showed higher fluorescence enhancement during incubation with  $\beta$ -sheet-rich A $\beta$  oligomers than incubation with unordered A $\beta$  oligomers. Triazole-containing dyes 25 and 26 showed high selectivity in the recognition of the ordered amyloid oligomers when compared to probes 23 and 24. In 2013, the same group reported 1,3,5,7-tetraphenyl-8-aza-BODIPY probe 27 [42] (Fig. 13). The fluorescence enhancement of conjugate 27 in the presence of ordered and unordered A $\beta$  oligomers was demonstrated in a PBS solution. However, this conjugate showed a 57-fold fluorescence increase in the presence of BSA, which is illustrative of the side hydrophobic interactions of this probe.

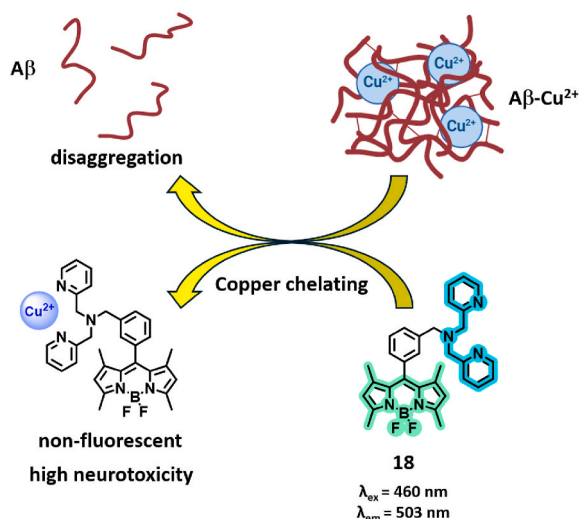


Fig. 9. BODIPY-based probe 18 with copper chelating dipicolylamine unit reported by Kong et al. [34].

High-throughput screening of libraries of potential drugs is often required to find a drug candidate with high-affinity. Thus, in 2015, Teoh et al. found an  $A\beta$  soluble oligomer-sensitive fluorescent probe by the diversity-oriented fluorescence library approach (DOFLA) among the library of 3500 fluorescent probes [64]. As a result, fluorescent probe 28 for  $A\beta$  oligomer detection was generated and synthesized [43] (Fig. 14). BODIPY 28 showed high selectivity for binding with  $A\beta$  soluble oligomers over other  $A\beta$  species. *In vivo* assays revealed the ability of probe 28 to penetrate BBB and selectively bind to  $A\beta$  oligomers by good colocalization with oligomer-specific 6E10/4G8 antibodies on APP/PS1 mouse brain samples.

Diphenylalanine motif recognition is of interest for early-stage AD diagnosis due to its key role in the  $A\beta$  self-assembling process [65]. With this in mind, Quan et al. designed a fluorescent probe 29 with an  $-NPh_2$  terminal rotor unit in the structure [45] (Fig. 15). Terminal diphenyl amino rotor was used with the idea that BODIPY 29 would fit into amyloid instead of diphenylalanine residue, thereby visualizing it. The ability of probe 29 to fit into nanofibrils was confirmed by SEM and

fluorescent imaging of aggregates obtained during the oligomerization of  $A\beta$  monomers in the presence of BODIPY 29. Probe 29 recognized self-assembled diphenylalanine nanofibrils at low concentrations ( $6.2 \times 10^{-5}$  M), while at a higher concentration ( $1 \times 10^{-3}$  M), conjugate 29 showed the ability to inhibit the self-assembling process. Selective binding of probe 29 with  $A\beta$  oligomers over both  $A\beta$  fibrils and

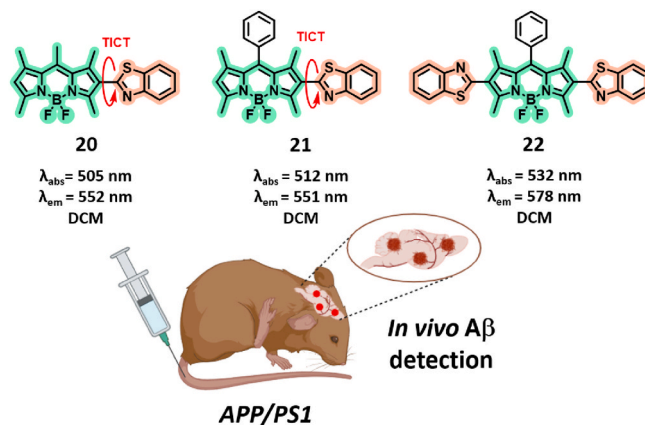


Fig. 11. BODIPY-based conjugates 20–22 both for  $A\beta$  binding and viscosity changes detection reported by Wang et al. [35].

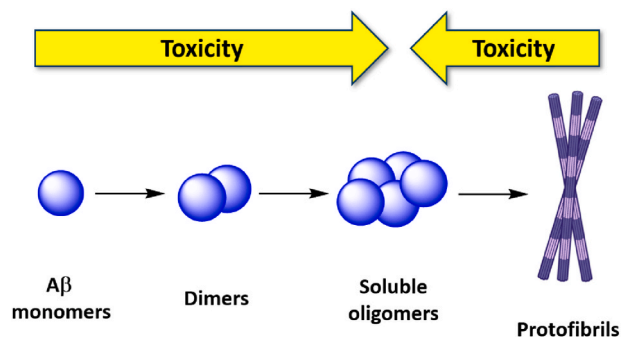


Fig. 12. Relative toxicity of different  $A\beta$  species [5].

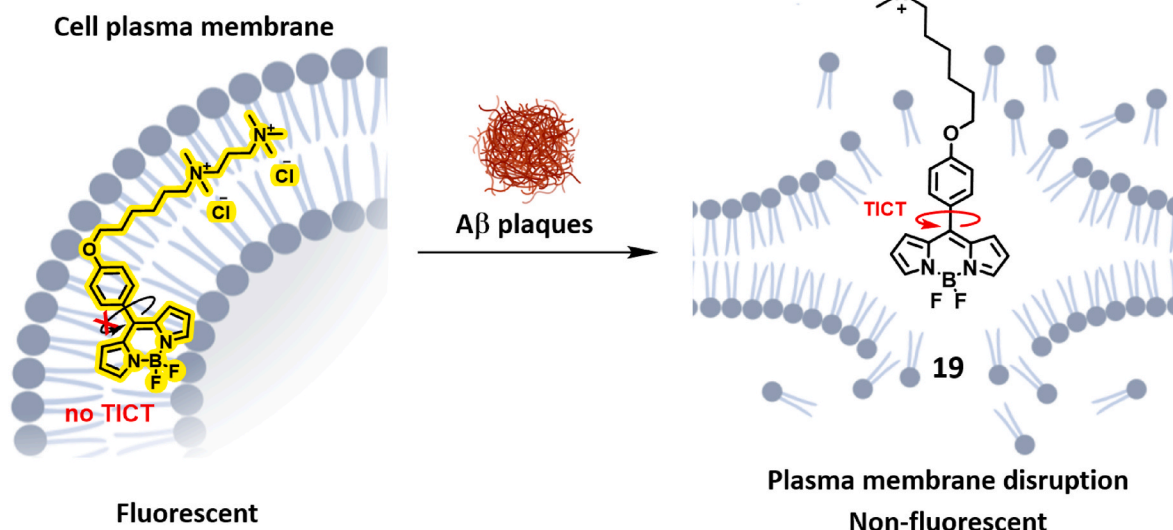


Fig. 10. Viscosity sensitive probe 19 for the determination of cell plasma membrane viscosity changes reported by Kubankova et al. [6].

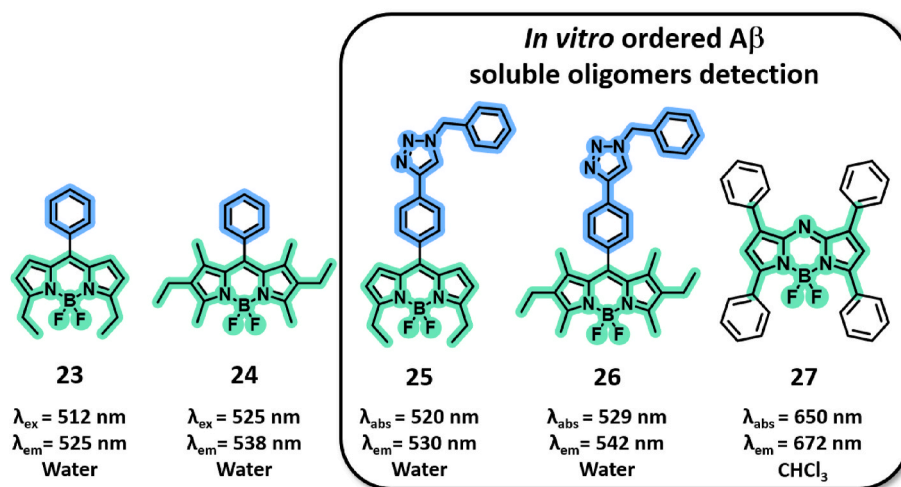


Fig. 13. BODIPY-based probes 23–27 for *in vitro* ordered A $\beta$  oligomer detection published by Smith et al. [41,42]. Photophysical data of the probe 27 from [43].

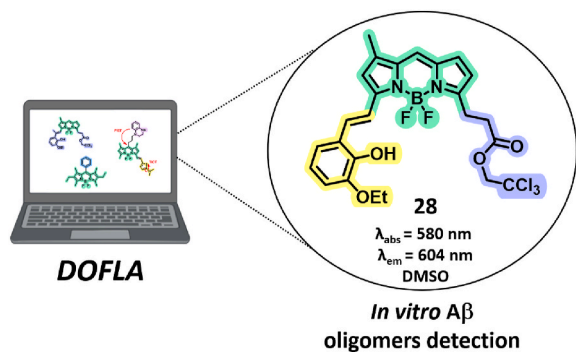


Fig. 14. BODIPY-based probe 28 reported by Teoh et al. [44].

monomers was proved by fluorescence emission measurements. BODIPY 29 demonstrated good co-localization with A $\beta$  oligomer specific antibodies A11 in *ex vivo* assays on cortex and hippocampus APP/PSEN1 mice and human brain slices. Low co-localization of probe 29 with A $\beta$  fibrillar oligomer specific antibodies OC proved high selectivity of the probe.

Another successful example of the use of computational methods in the search for a high-affinity molecule satisfying certain parameters was

reported by Ono et al. in 2023 [46]. A SAR study of BODIPY derivatives revealed 17 BAP-1-based fluorescent probes 30–46 for selective A $\beta$  oligomer detection (Fig. 16). Among others,  $\gamma$ -shaped BODIPY-based probe 45 showed 1.2-fold fluorescence enhancement selectivity for binding with A $\beta$  oligomers over fibrils higher than PTO-41, an A $\beta$  oligomer-selective probe reported previously [66]. Also, probe 45 showed good colocalization with A $\beta$  oligomer specific antibodies (OMAB) on APP<sup>NL-G-F/NL-G-F</sup> mouse brain sections. Moreover, a slight difference in fluorescent signal between AD and normal mice was observed *in vivo* in spite of low brain uptake (0.43 % ID/g at 2 min p.i.) of radiolabeled conjugate [<sup>18</sup>F]45.

#### 4.6. BODIPY-based probes for intraneuronal neurofibrillary tangles (NFTs) detection

Tau is a protein that is present in neuronal cells; the binding of tau to microtubules is primarily regulated by serine/threonine-directed phosphorylations. Under pathological conditions, tau is abnormally hyperphosphorylated at more than 30 sites, loses its binding ability, and accumulates in brain tissue as insoluble filamentous aggregates [67]. Hexapeptide PHF6 (Paired Helical Filament 6) with the sequence <sup>306</sup>VQIVYK<sup>311</sup> is responsible for tau protein aggregation [68]. Rational design of selective tau imaging agents is a challenging task, which is the subject of a significant number of publications [69].

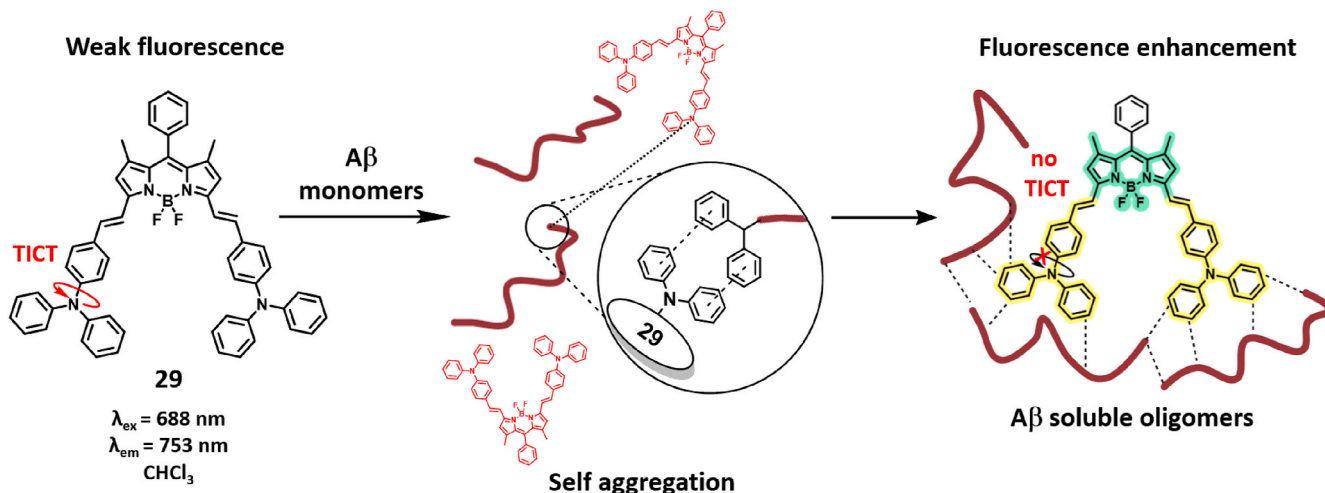


Fig. 15. BODIPY-based probe 29 reported by Quan et al. [45].

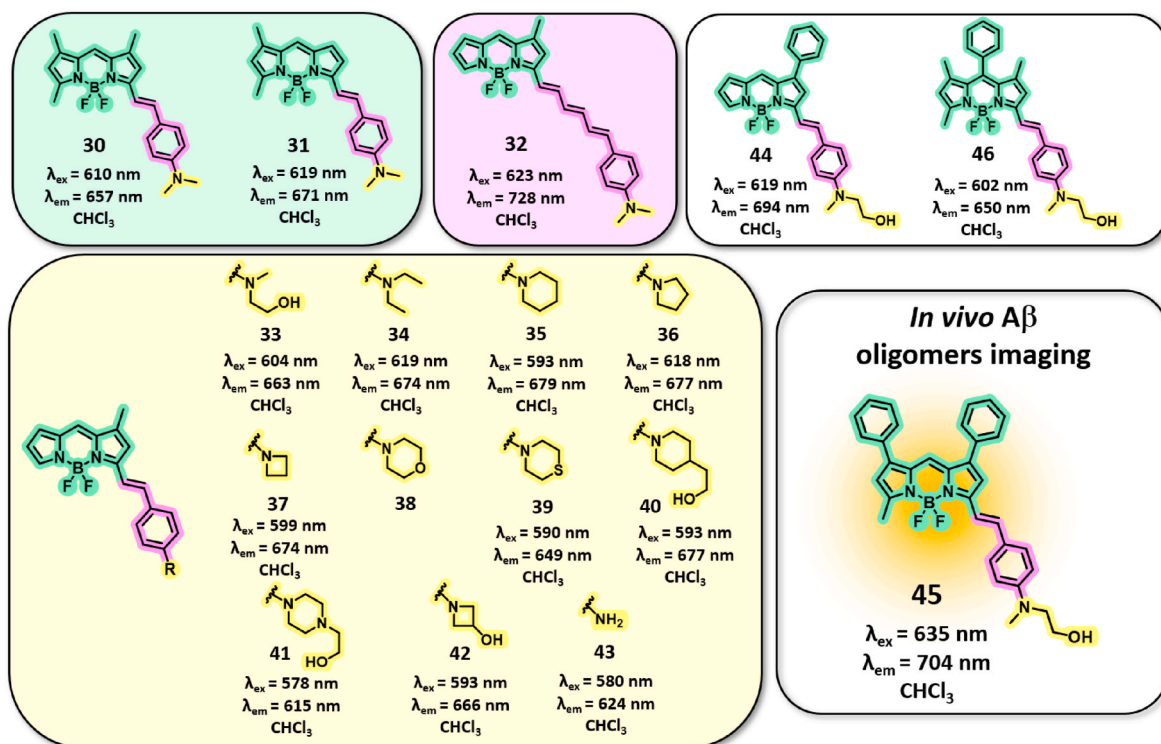


Fig. 16. BODIPY derivatives for A $\beta$  oligomers *in vivo* visualization 30–46 published by Ono et al. [46] No photophysical data for probe 38 is given.

For selective recognition and sensing of phosphorylated proteins, a binuclear Zn(II)-dipicolylamine (DPA)-bipyridyl complex capable of bis-phosphorylated peptide binding in a cross-linking manner was proposed by Hamachi et al. [70,71]. Later in 2009, a BODIPY-based probe based on the Zn(II)-DPA complex for the fluorescence detection of hyperphosphorylated tau protein was proposed by Ojida et al. (Fig. 17) [23]. In the molecular design of probes 47 and 48, the two Zn(II)-DPA units were conjugated directly to the BODIPY moiety to provide the system with a planar and rigid conformation, capable of strong interactions with the  $\beta$ -sheet-rich structure of the NFTs. Triethylene glycol chains were used for their high solubility in aqueous solutions. The resulting

BODIPY 47 showed binding ability with several bisphosphorylated  $\tau$ -proteins by interaction between Zn ions and orthophosphoric acid residues with concentration-dependent fluorescence enhancement. On the other hand, fluorescence titration of mononuclear complex 48 with similar proteins did not show such an increase. The binding selectivity of BODIPY 47 with aggregates of tau-phosphorylated protein (pTau) over the binding with normal tau-protein aggregates and A $\beta$  fibrils was shown by the fluorescent titration method. Fluorescence enhancement of probe 47 was not observed in the presence of normal tau-protein aggregates and A $\beta$  species. Also, *in vitro* staining with hippocampus tissue sections from AD patients showed high co-localization of

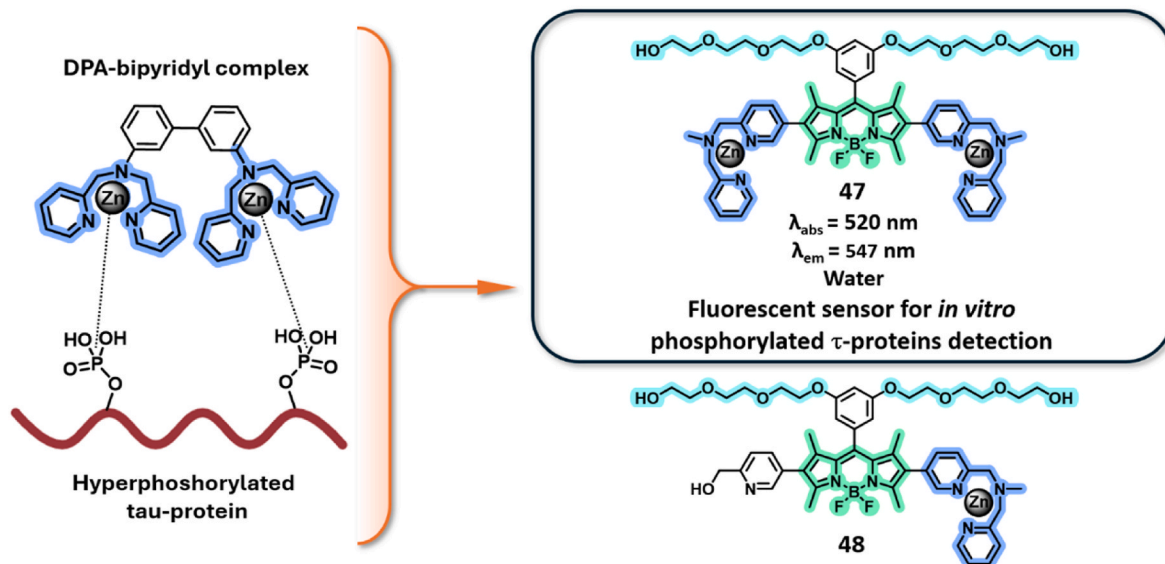


Fig. 17. Zn(II)-DPA-bipyridyl complex capable of bis-phosphorylated peptide binding reported by Hamachi et al. [70], and BODIPY-DPA-Zn complexes 47 and 48 for *in vitro* NFT visualization reported by Ojida et al. [23].

conjugate **47** with pTau-specific antibodies AT8.

To date, two hypotheses guide the design of NFT-binding drugs. According to the first, in D-A fluorescent probes, a distance between the donor and acceptor parts of 13–19 Å benefits NFT selectivity, whereas shorter distances favor A $\beta$  plaques; according to the second, fused ring systems contribute to tau binding selectivity over A $\beta$  fibrils [24,72,73]. Taking these hypotheses as a design basis, Verwilt et al. designed an NFT-selective probe based on BAP-1 **49** and **50** with different styryl groups [24] (Fig. 18). BODIPY **49** and **50** were designed to maintain the required distance between the *meso*-position of the BODIPY core and the donor nitrogen atom, which was confirmed by DFT calculations. Docking studies revealed the ability of probes **49** and **50** to bind with the R3 microtubule binding region of the PHF6 peptide sequence. Both BODIPYs **49** and **50** demonstrated fluorescence increases in the presence of tau protein aggregates, while incubation with A $\beta$  aggregates led to insignificant probes' **49** and **50** quantum yield increases. Cytotoxicity of conjugates **49** and **50** was not observed on SKNMC, U87, SH-SY5Y, C6, and N2A cell lines. Furthermore, the ability to detect NFTs *in vitro* was confirmed by the fluorescence enhancement of probes **49** and **50** on SH-SY5 cells during incubation with okadaic acid, which promotes protein phosphorylation [74]. *In vivo* studies on 3xTg mice revealed the BBB penetration ability of probe **49** and its selective binding to NFTs in further *ex vivo* fluorescence staining experiments. Moreover, BODIPY **49** was able to detect NFTs with IVIS by detecting a significant increase in fluorescent signal intensity at 30 min p.i.

The high cell-permeability property of the BODIPY core leads to the widespread use of the BODIPY scaffold as a basis for intracellular fluorescent probes [75–77]. Given this, the development of fluorescent probes capable of intracellular detection of Tau protein is an extremely interesting task, especially considering the impermeability of the cell membrane to “gold standard” ThS. This task was resolved in 2017 by Lim et al. via the reporting of a BODIPY-chloroacetamide-based cell-permeable probe **51** for intracellular NFT detection [25] (Fig. 19). Conjugates **51** and **52** were designed by DOFLA and demonstrated high selectivity for NFTs over interaction with tau protein aggregates and pre-aggregates *via* fluorescence enhancement. BODIPY **51**, unlike **52**, showed high affinity to NFT over BSA, actin, and glyceraldehyde 3-phosphate dehydrogenase; selectivity for tau-aggregate binding in hippocampal neuronal HT22 cells was also shown. High Tau selectivity of BODIPY **51** was demonstrated in HEK293 Tau-BIFC cells pre-treated with forskolin, which induces tau protein aggregation. Also, high

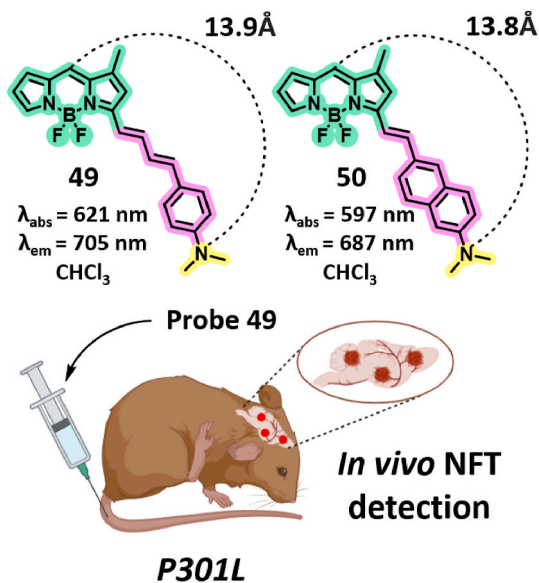


Fig. 18. BODIPY-based probes **49** and **50** for selective fluorescence detection of NFT published by Verwilt et al. [24].

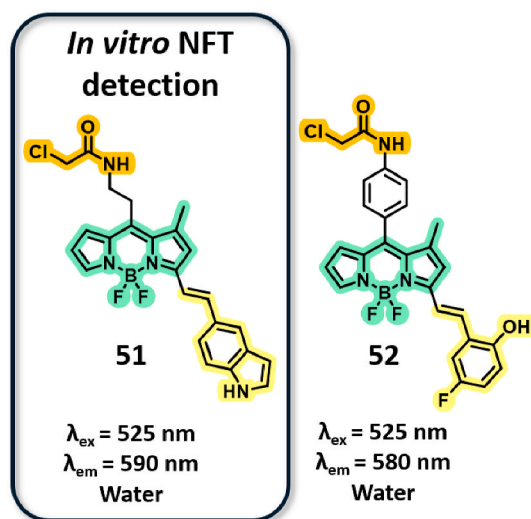


Fig. 19. BODIPY-based probes **51** and **52** for selective *in vitro* NFT visualization reported by Lim et al. [25].

co-localization of BODIPY **51** and anti-tau PHF antibodies was demonstrated *ex vivo* on MAPT\*P301L brain tissue sections.

In 2017, Mani et al. designed ten fluorescent BODIPY-*p*-methoxyphenyl derivatives **53–62** with different  $\pi$ -conjugated systems in the 3-rd position of the BODIPY core for real-time tracking of *in vitro* aggregation of tau [26] (Fig. 20). Probe **61** showed the highest fluorescence enhancement upon binding to NFTs and the largest Stock's shift value. Also, BODIPY **61** showed low cytotoxicity and high cellular uptake in HeLa cells. However, a fluorescence staining experiment demonstrated that BODIPY **61** binds to terminal units only, thus indicating its low prospects for the quantitative determination of Tau protein. However, probe **61** is cell membrane permeable (unlike ThT), which makes it a promising scaffold for the development of intracellular probes for monitoring tau protein aggregation.

Since BODIPYs **49** and **50** showed the ability to successfully visualize NFTs, their molecular scaffold was used as the basis for other Tau-selective fluorescent probes. In an attempt to improve the photo-physical properties of BODIPY **49** and **50**, Xie et al. used Knoevenagel condensation of a *meso*-methyl group of BODIPY with *N*-dimethylamino-substituted aromatic aldehydes have different lengths of C=C units. However, 1,4-Michael addition of the BODIPY enolate took place, followed by cyclization of the cycloheptatriene ring, yielding six heptacyclotriene-BODIPY probes **63–67** [27] (Fig. 21). Probes **64**, **65**, **67**, and **68** exhibited better affinity to Tau-K18 aggregates and higher fluorescence ignition in comparison with BODIPYs **63** and **66**. *In vitro* studies demonstrated the high selectivity of probes' **64**, **65**, **67**, and **68** binding with NFTs over A $\beta$  species on human brain samples. *In vivo* experiments with BABL/c mice showed high BODIPYs **64** and **67** brain uptake and rapid washout from WT mouse brain tissue. However, probe **64** demonstrated only a slight fluorescence intensity difference among the P301L Tg and WT mice groups detected by IVIS.

As a follow-up to this study, Li et al. further optimized the sample structure and reported another series of cycloheptatriene BODIPY derivatives **69–75** with rotor units modified with a 2-hydroxyethyl moiety [47] (Fig. 22). The highest affinity for Tau-K18 $\Delta$ 280 was observed for conjugates **70**, **73**, and **75**. Also, probes **70**, **73**, and **75** exhibited the highest selectivity of fluorescence enhancement upon binding with NFTs over A $\beta$  species. *Ex vivo* studies confirmed probes' **70**, **73**, and **75** binding selectivity by high co-localization with AT-8 and Gallays-Braak positive regions and their low concordance with the A $\beta$ -specific DANIR 3b fluorescent pattern on human brain samples. *In vivo* experiments on BABL/c mice proved the ability of BODIPYs **70** and **73** to penetrate the BBB and their rapid washout from brain tissue.

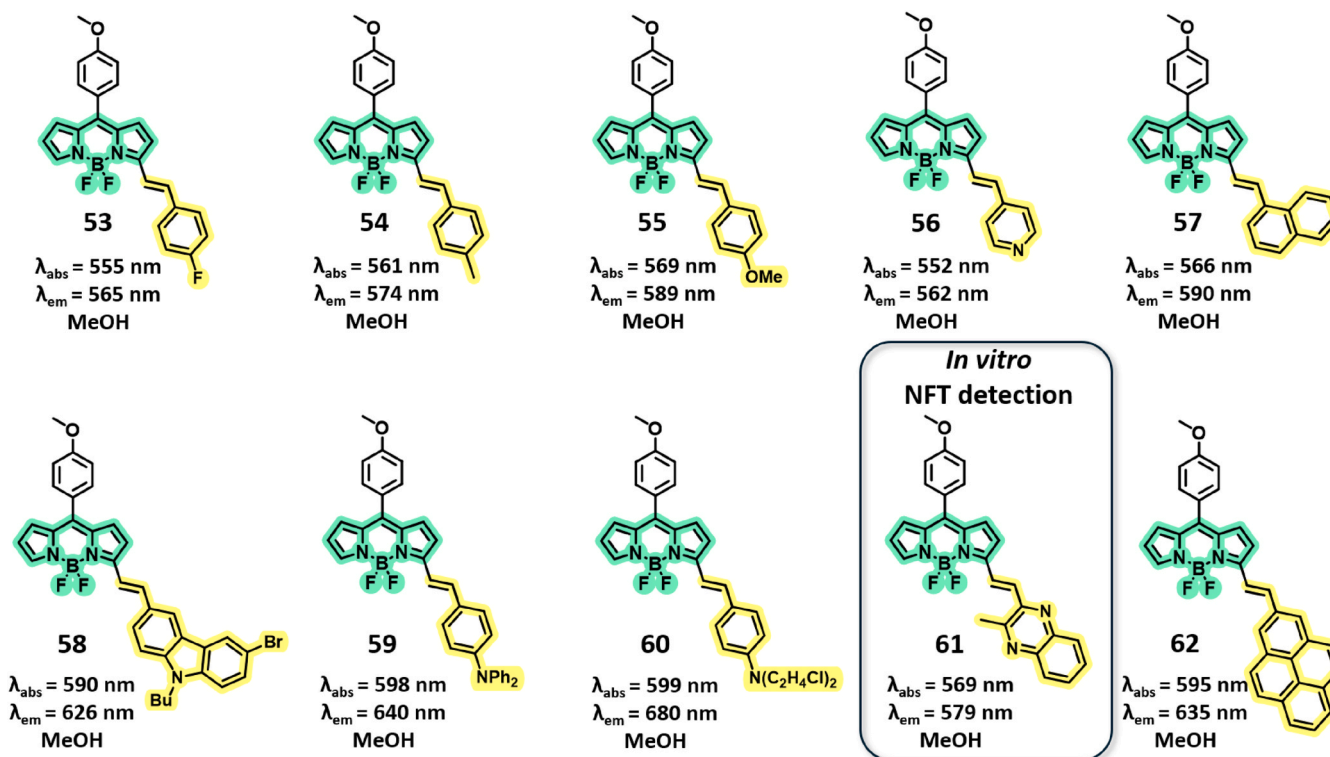
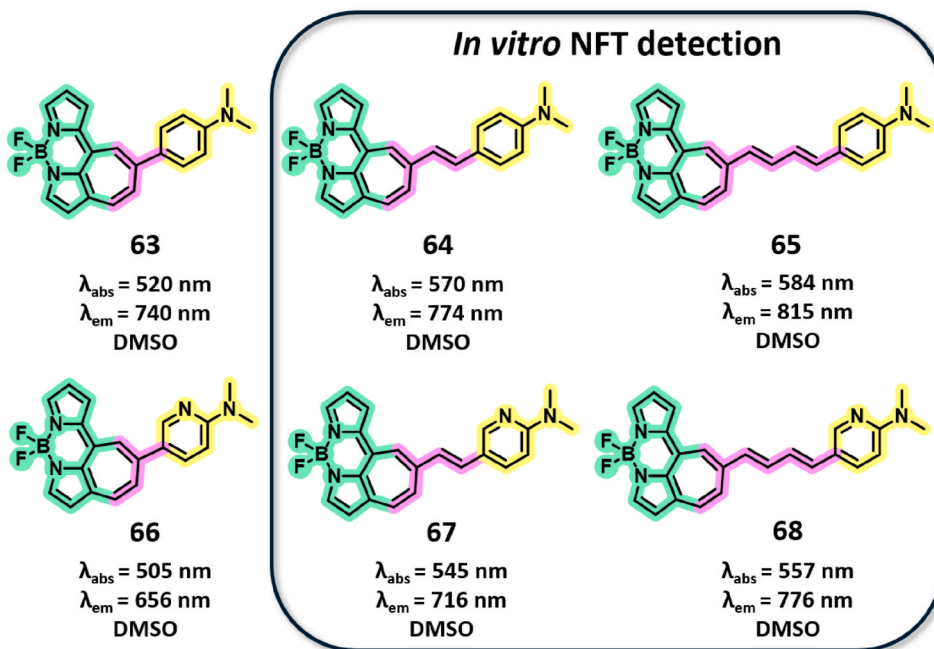


Fig. 20. Fluorescent probes for NFT detection 53–62 published by Mani et al. [26].

Fig. 21. BODIPY derivatives 63–68 for *in vivo* NFT visualization published by Xie et al. [27].

## 5. Discussion

Fluorescence imaging of pathologic changes in AD patients shows undeniable advantages over clinically used SPECT, PET, and MRI techniques due to their high sensitivity, high resolution, low cost, and non-invasiveness [11]. Even though optical visualization is also limited by significant background interference and poor tissue penetration [19], this method offers real-time non-invasive and non-radiative A $\beta$  and NFT

visualization, thus making the development of fluorescent probes an extremely promising strategy for AD diagnostic. In the past decade, the development of fluorescent probes for the detection of AD hallmarks has been a relevant task. Most fluorescent probes were developed for A $\beta$  plaque mapping, while probes capable of soluble oligomers, NFTs, and other AD-related therapeutic targets visualization are worse represented.

To date, most reported probes for the detection of A $\beta$  plaques are

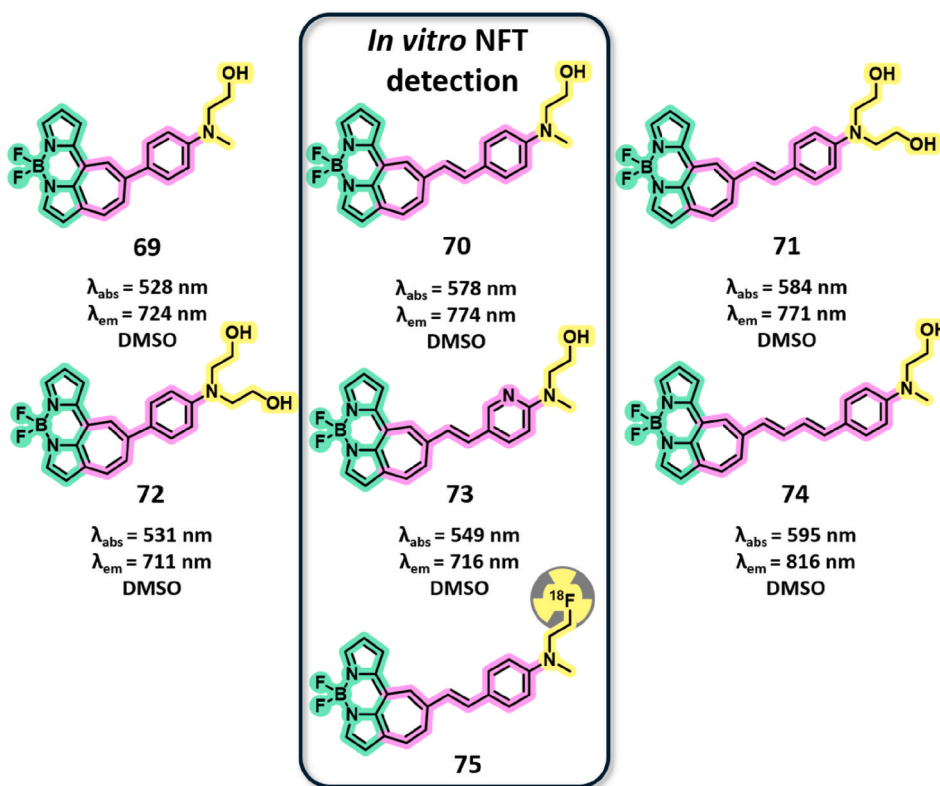


Fig. 22. BODIPY-based probes 69–74 for *in vivo* NFT fluorescence visualization and radiolabeled conjugate 75 for PET imaging of NFTs reported by Li et al. [47].

based on a donor– $\pi$ –acceptor structure with a PIET or ICT-based fluorescence quenching mechanism [29,30,36]. TICT-based probes exhibit weak fluorescence in their free state due to the free rotation of molecule fragments relative to each other, resulting in energy dissipation and non-emissive relaxation; upon binding with biomolecules, restriction of probe conformational motion leads to an increase in fluorescence [49, 50].

A TICT fluorescence quenching mechanism was used to develop fluorescent BODIPY-based probes 1–15 for the detection of A $\beta$  plaques [28–33]. Probes 1–3 were the first to demonstrate the ability to selectively bind to A $\beta$  aggregates *in vitro*, and probes 2 and 3 (known as BAP-1 and BAP-2), not applicable for optical detection of A $\beta$  *in vivo* due to accumulation in the mouse scalp, still serve as inspiration and molecular scaffolds for A $\beta$ -targeted drug design [28–30]. Thus, BODIPYs 13 and 15 developed based on 1 and 2 demonstrated successful visualization of A $\beta$  plaques *in vivo* [29,30]. However, the high sensitivity of TICT-based probes for hydrophobic environments significantly limits their application for *in vivo* imaging. Thus, another approach to fluorescent probe design based on a less-sensitive PIET fluorescence quenching mechanism was suggested. This method was applied to design probes 16a and 17 for A $\beta$  plaque detection [36,40]. Probe 16a demonstrated the ability of *in vitro* A $\beta$  visualization on brain samples without a prewashing procedure, thus illustrating a low level of side interactions compared to the TICT-based analogues and high selectivity [40]. Further modification of probe 16 with a dimethylamino-thiophene moiety yielded BODIPY 17, which successfully visualized A $\beta$  plaques *in vivo* [36].

Copper ions are well-known to be involved in the pathogenesis of AD; metal dyshomeostasis in brain tissue, the formation of Cu-A $\beta$  aggregates, and the resulting oxidative stress are therapeutic targets in the development of anti-AD drugs. Thus, fluorescent probes with copper chelators are of interest for both AD therapeutic and diagnostic purposes. Copper-chelating probe 18 showed the ability to disaggregate beta-amyloid plaques, but the high neurotoxicity of Cu-18 complexes limited the further study of its efficacy *in vivo* [34].

A $\beta$  species are also well-known to promote oxidative damage to brain tissue cells, which results in cell membrane rupture and changes in intracellular medium viscosity [6,78]. Thus, molecular rotors were assumed to be applicable for AD diagnosis as viscosity-sensitive fluorophores [6,35]. Probes 20 and 21 demonstrated their potential for *in vitro* imaging of A $\beta$  plaques, *in vivo* studies of BODIPY 20 showed a difference in fluorescence between APP/PS1 and WT mice [35].

A $\beta$  oligomers are considered the most neurotoxic aggregates among other A $\beta$  species, playing a key role in the progression of AD. Thus, *in vitro* detection of A $\beta$  oligomers might be applied for AD patients' assessment and early-stage diagnosis [59]. BODIPYs 23–46 were designed as probes for A $\beta$  oligomer detection [41–46]. Among others, probes 28, 29, and 45 showed the ability to detect A $\beta$  oligomers *in vitro*. BODIPY 29 showed the ability to bind with diphenylalanine residue by fitting into the A $\beta$  oligomer structure during the self-assembling process, thus proving the prospects diphenyl amino rotor unit applications for AD diagnosis [45]. BODIPY 45 showed an ability for *in vivo* detection of A $\beta$  oligomers, with a slight difference in fluorescence between AD and WT mice *in vivo* [43–46]. It should be especially noted that the y-form of BODIPY's 45 molecule differs from the previously proposed T- and V-forms that can fit into a triangular cavity; an y-form can also be considered promising for binding to A $\beta$  oligomers.

BODIPYs 47–75 were developed for the detection of such essential AD hallmarks as NFTs [23–27,47]. Even though probes 47, 49, 50, 51, 64, 65, 67, 68, 70, 73, and 75 were capable of selective NFT visualization *in vitro*, only probe 49 showed a clear difference in fluorescence between AD and WT mice *in vivo* [23–27,47]. Despite the large number of probes designed for NFT detection, only BODIPY 49 showed the ability to detect them *in vivo*. Comparison of NFT visualization probes also showed that the distance between the terminal rotor fragment and the BODIPY core is crucial, with the optimal value being 13–19 Å [24].

Thus, despite the prevalence of TICT-based probes for A $\beta$  detection, this kind of fluorophores is extremely sensitive for hydrophobic environments, which could trigger their fluorescence. Besides, BODIPYs with

a PIET-based fluorescence quenching mechanism are less sensitive to surrounding polarities, representing a more desirable direction for the development of probes for AD species visualization *in vivo*. TICT-based probes for A $\beta$  detection **33–43** showed that substitution of the rotor unit could affect the selectivity of the probe and its fluorescence quenching, but no pattern of this effect was observed [46]. It is also worth noting that probes **13**, **15**, **20**, and **45**, which showed the ability to detect A $\beta$  species *in vivo*, represent structures substituted at the 5th and 7th positions of the BODIPY core [32,33,35,46].

## 6. Conclusion

Optical imaging is an extremely promising technique for AD diagnosis development due to its low cost, high sensitivity, high resolution, and non-invasiveness. BODIPY dyes, due to unique photophysical properties, the possibility of easy modification, high chemical and photostability are excellent motifs for the design of diagnostic agents for the visualization of various AD-related species *in vivo*. Thus, TICT-based BODIPY conjugates modified with styryl units demonstrated the ability to detect A $\beta$  plaques *in vitro*, BODIPY **13** and **15** showed the ability to visualize A $\beta$  aggregates *in vivo*, presumably due to the presence of methyl or phenyl groups at the 5-th and 7-th positions of the BODIPY core. Moreover, PIET-based BODIPYs **16** and **17** showed a much lower level of background fluorescent signal in comparison with TICT-based analogues *in vitro*, and probe **17** was capable of A $\beta$  plaque detection *in vivo*. Moreover, probe **29** demonstrated the ability to bind with diphenylalanine residue, which is responsible for A $\beta$  monomer aggregation, thus, making the diphenyl amine rotor unit an extremely promising moiety both for AD diagnosis agents' development and A $\beta$  oligomerization process visualization. TICT-based BODIPY probe **45** was successfully developed for A $\beta$ -soluble oligomers *in vivo* detection by varying the rotor unit and positions of substituents at the BODIPY core.

BODIPY-based dyes with TICT fluorescence quenching mechanisms showed the ability to detect NFTs *in vivo*. The modern design is based on two hypotheses that “fused-ring” units increase the selectivity for tau-protein aggregates over A $\beta$  species, and that the distance between donor and acceptor molecule parts is crucial, with the optimal value being 13–19 Å. Probe **49** demonstrated the ability of NFT for *in vivo* visualization, thus proving the applicability of design proposed.

The design of a fluorescent probe that can efficiently cross the BBB, selectively bind to a target, and produce a meaningful response requires thoughtful and careful consideration. Molar mass, Stokes's shift, absorption and emission of the fluorophore, photophysical aspect of the fluorescent response, mechanism of binding to the protein target, ability to form hydrogen bonds, and shape of the molecule must be taken into account. The successful images of AD's hallmarks presented in this review show the promise of BODIPY for fluorescent visualization for AD-related brain pathologies.

## CRedit authorship contribution statement

**Daniil Abramchuk**: Writing – original draft. **Alevtina Voskresenskaya**: Writing – review & editing. **Ilia Kuzmichev**: Writing – review & editing. **Alexander Erofeev**: Funding acquisition. **Peter Gorelkin**: Project administration. **Maxim Abakumov**: Project administration. **Elena Beloglazkina**: Conceptualization. **Olga Krasnovskaya**: Writing – original draft, Visualization, Supervision, Data curation, Conceptualization.

## Declaration of competing interest

The authors declare the following financial interests/personal relationships which may be considered as potential competing interests: Alexander Erofeev reports financial support was provided by National University of Science and Technology MISIS. Olga Krasnovskaya reports a relationship with National University of Science and Technology MISIS

that includes: employment. There is no conflict of interest to declare. If there are other authors, they declare that they have no known competing financial interests or personal relationships that could have appeared to influence the work reported in this paper.

## Data availability

No data was used for the research described in the article.

## Acknowledgement

The work was financially supported by the Ministry of Science and Higher Education of the Russian Federation, Agreement No. 075-15-2022-264 (unique scientific facility “Scanning ion-conductance microscope with a confocal module”, registration number 2512530).

## List of abbreviations

A $\beta$	–	beta amyloid
AChE	–	acetylcholinesterase
AD	–	Alzheimer's disease
BBB	–	blood–brain barrier
BODIPY	–	4,4-difluoro-4-bora-3a,4a-diaza-s-indacene
BSA	–	bovine serum albumin
DFT	–	density functional theory
DOFLA	–	diversity oriented fluorescence library approach
DPA	–	dipicalyl amine
GPMV	–	giant plasma membrane vesicles
HOMO	–	highest occupied molecular orbital
HSA	–	human serum albumin
ICT	–	intramolecular charge transfer
IVIS	–	<i>in vivo</i> imaging system
LUMO	–	lowest unoccupied molecular orbital
MRI	–	magnetic resonance imaging
MTT	–	microtiter plate
NFT	–	neurofibrillary tangles
NIR	–	near-infrared
PET	–	positron emission tomography
PIET	–	photoinduced electron transfer
pTau	–	phosphorylated tau-proteins
ROS	–	reactive oxygen species
SAR	–	structure-active relationship
SEM	–	scanning electron microscopy
SPECT	–	single-photon emission computed tomography
TDDFT	–	time-dependent density functional theory
TEM	–	transmission electron microscopy
Tg	–	transgenic
TICT	–	twisted intramolecular charge transfer
ThS	–	Thioflavin S
ThT	–	Thioflavin T
WT	–	wild-type

## References

- [1] X. Li, X. Feng, X. Sun, N. Hou, F. Han, Y. Liu, Global, regional, and national burden of Alzheimer's disease and other dementias, 1990–2019, *Front. Aging Neurosci.* 14 (2022) 937486.
- [2] J. Rasmussen, H. Langerman, Alzheimer's disease—why we need early diagnosis, *Degener. Neurol. Neuromuscul. Dis.* (2019) 123–130.
- [3] Z.X. Wang, L. Tan, J. Liu, J.T. Yu, The essential role of soluble A $\beta$  oligomers in Alzheimer's disease, *Mol. Neurobiol.* 53 (2016) 1905–1924.
- [4] L. Liu, H. Kwak, T.L. Lawton, S. Jin, A.L. Meunier, Y. Dang, B. Ostaszewski, A. C. Pietras, A.M. Stern, D.J. Selkoe, An ultra-sensitive immunoassay detects and quantifies soluble A $\beta$  oligomers in human plasma, *Alzheimer's Dementia* 18 (2022) 1186–1202.
- [5] M. Habashia, S. Vutlab, K. Tripathia, S. Senapatia, P.S. Chauhanb, A. Haviv-Chesnera, M.I. Richmana, S. Mohandc, V. Dumulon-Perreaultd, R. Mulamreddyb, E. Okune, J.H. Chilla, B. Guerinc, W.D. Lubellb, S. Rahimpour, Early diagnosis and

- treatment of Alzheimer's disease by targeting toxic soluble A $\beta$  oligomers, *Proc. Natl. Acad. Sci. U.S.A.* 119 (2022) e2210766119.
- [6] M. Kubánková, I. López-Duarte, D. Kiryushko, M.K. Kuimova, Molecular rotors report on changes in live cell plasma membrane microviscosity upon interaction with beta-amyloid aggregates, *Soft Matter* 14 (2018) 9466–9474.
- [7] P. Zatta, D. Drago, S. Bolognin, S.L. Sensi, Alzheimer's disease, metal ions and metal homeostatic therapy, *Trends Pharmacol. Sci.* 30 (2009) 346–355.
- [8] V. Valotassiou, J. Malamitsi, J. Papatriantafyllou, E. Dardiotis, I. Tsougos, D. Psimadas, S. Alexiou, G. Hadjigeorgiou, P. Georgoulas, SPECT and PET imaging in Alzheimer's disease, *Ann. Nucl. Med.* 32 (2018) 583–593.
- [9] R. Ni, Magnetic resonance imaging in animal models of Alzheimer's disease amyloidosis, *Int. J. Mol. Sci.* 22 (2021) 12768.
- [10] O. Krasnovskaya, A. Kononova, A. Erofeev, P. Gorelkin, A. Majouga, E. Beloglazkina, A $\beta$ -targeting bifunctional chelators (BFCs) for potential therapeutic and PET imaging applications, *Int. J. Mol. Sci.* 24 (2023) 236.
- [11] O. Krasnovskaya, D. Spector, A. Zlobin, K. Pavlov, P. Gorelkin, A. Erofeev, E. Beloglazkina, A. Majouga, Metals in imaging of alzheimer's disease, *Int. J. Mol. Sci.* 21 (2020) 1–35.
- [12] T.E. Golde, B.J. Bacskai, Bringing amyloid into focus, *Nat. Biotechnol.* 23 (2005) 552–554.
- [13] M. Staderini, M.A. Martín, M.L. Bolognesi, J.C. Menéndez, Imaging of  $\beta$ -amyloid plaques by near infrared fluorescent tracers: a new frontier for chemical neuroscience, *Chem. Soc. Rev.* 44 (2015) 1807–1819.
- [14] D. Su, W. Diao, J. Li, L. Pan, X. Zhang, X. Wu, W. Mao, Strategic design of amyloid- $\beta$  species fluorescent probes for alzheimer's disease, *ACS Chem. Neurosci.* 13 (2022) 540–551.
- [15] J. Zhou, P. Jangili, S. Son, M.S. Ji, M. Won, J.S. Kim, Fluorescent diagnostic probes in neurodegenerative diseases, *Adv. Mater.* 32 (2020) 1–43.
- [16] Z.Y. Zhang, Z.J. Li, Y.H. Tang, L. Xu, D.T. Zhang, T.Y. Qin, Y.L. Wang, Recent research progress in fluorescent probes for detection of amyloid- $\beta$  in vivo, *Biosensors* 13 (2023) 1–16.
- [17] J. Yang, F. Zeng, Y. Ge, K. Peng, X. Li, Y. Li, Y. Xu, Development of near-infrared fluorescent probes for use in alzheimer's disease diagnosis, *Bioconjugate Chem.* 31 (2020) 2–15.
- [18] Y.I. Gyasi, Y.P. Pang, X.R. Li, J.X. Gu, X.J. Cheng, J. Liu, T. Xu, Y. Liu, Biological applications of near infrared fluorescence dye probes in monitoring Alzheimer's disease, *Eur. J. Med. Chem.* 187 (2020) 111982.
- [19] J. Yang, Y. Guo, M. Pistolozzi, J. Yan, Research progress of multi-functional fluorescent probes for Alzheimer's disease monitoring, *Dyes Pigments* 193 (2021) 109466.
- [20] M. Poddar, R. Misra, Recent advances of BODIPY based derivatives for optoelectronic applications, *Coord. Chem. Rev.* 421 (2020) 213462.
- [21] P.K. Singh, P. Majumdar, S.P. Singh, Advances in BODIPY photocleavable protecting groups, *Coord. Chem. Rev.* 449 (2021) 214193.
- [22] M. Ahmed, N. Mushtaq, N. Sher, R.A. Khan, M.A. Masood, The therapeutic effect of BODIPY-based photosensitizers against acetylcholinesterase for the treatment of Alzheimer's disease, *J. Prot. Proteom.* (2024) 1–5.
- [23] A. Ojida, T. Sakamoto, M.A. Inoue, S.H. Fujishima, G. Lippens, I. Hamachi, Fluorescent BODIPY-based Zn(II) complex as a molecular probe for selective detection of neurofibrillary tangles in the brains of alzheimer's disease patients, *J. Am. Chem. Soc.* 131 (2009) 6543–6548.
- [24] P. Verwilt, H.R. Kim, J. Seo, N.W. Sohn, S.Y. Cha, Y. Kim, S. Maeng, J.W. Shin, J. H. Kwak, C. Kang, J.S. Kim, Rational design of in vivo tau tangle-selective near-infrared fluorophores: expanding the BODIPY universe, *J. Am. Chem. Soc.* 139 (2017) 13393–13403.
- [25] S. Lim, M.M. Haque, D. Su, D. Kim, J.S. Lee, Y.T. Chang, Y.K. Kim, Development of a BODIPY-based fluorescent probe for imaging pathological tau aggregates in live cells, *Chem. Commun.* 53 (2017) 1607–1610.
- [26] V. Mani, V.G. Krishnakumar, S. Gupta, S. Mori, I. Gupta, Synthesis and characterization of styryl-BODIPY derivatives for monitoring in vitro Tau aggregation, *Sensor. Actuator. B Chem.* 244 (2017) 673–683.
- [27] T. Xie, Y. Li, C. Tian, C. Yuan, B. Dai, S. Wang, K. Zhou, J. Liu, H. Tan, Y. Liang, J. Dai, B. Chen, M. Cui, Fused cycloheptatriene-BODIPY is a high-performance near-infrared probe to image tau tangles, *J. Med. Chem.* 65 (2022) 14527–14538.
- [28] M. Ono, M. Ishikawa, H. Kimura, S. Hayashi, K. Matsumura, H. Watanabe, Y. Shimizu, Y. Cheng, M. Cui, H. Kawashima, H. Saji, Development of dual functional SPECT/fluorescent probes for imaging cerebral  $\beta$ -amyloid plaques, *Bioorg. Med. Chem. Lett* 20 (2010) 3885–3888.
- [29] M. Ono, H. Watanabe, H. Kimura, H. Saji, BODIPY-based molecular probe for imaging of cerebral  $\beta$ -amyloid plaques, *ACS Chem. Neurosci.* 3 (2012) 319–324.
- [30] H. Watanabe, M. Ono, K. Matsumura, M. Yoshimura, H. Kimura, H. Saji, Molecular imaging of  $\beta$ -amyloid plaques with near-infrared boron dipyrromethane (BODIPY)-based fluorescent probes, *Mol. Imag.* 12 (2013) 338–347.
- [31] F. Sozmen, S. Kolemen, H.O. Kumada, M. Ono, H. Saji, E.U. Akkaya, Designing BODIPY-based probes for fluorescence imaging of  $\beta$ -amyloid plaques, *RSC Adv.* 4 (2014) 51032–51037.
- [32] L. Ma, Y. Geng, G. Zhang, Z. Hu, T.D. James, X. Wang, Z. Wang, Near-infrared bodipy-based molecular rotors for  $\beta$ -amyloid imaging in vivo, *Adv. Healthcare Mater.* 12 (2023) 2300733.
- [33] M. Zhu, G. Zhang, Z. Hu, C. Zhu, Y. Chen, T.D. James, L. Ma, Z. Wang, A BODIPY-based probe for amyloid- $\beta$  imaging in vivo, *Org. Chem. Front.* 10 (2023) 1903–1909.
- [34] M.Y. Kong, Q.Y. Chen, L. Yao, Y.B. Wang, Spectroscopic study on the interaction of A $\beta$ 42 with di(picolyl)amine derivatives and the toxicity to SH-SY5Y cells, *Spectrochim. Acta Part A Mol. Biomol. Spectrosc.* 138 (2015) 225–228.
- [35] Y. Wang, J. Yang, Q. Chen, J. Su, W.J. Shi, L. Zhang, C. Xia, J. Yan, Rotor-tuning boron dipyrromethenes for dual-functional imaging of A $\beta$  oligomers and viscosity, *ACS Appl. Bio Mater.* 5 (2022) 3049–3056.
- [36] W. Ren, J. Zhang, C. Peng, H. Xiang, J. Chen, C. Peng, W. Zhu, R. Huang, H. Zhang, Y. Hu, Fluorescent imaging of  $\beta$ -amyloid using BODIPY based near-infrared off-on fluorescent probe, *Bioconjugate Chem.* 29 (2018) 3459–3466.
- [37] S.V. Dzzyuba, BODIPY dyes as probes and sensors to study amyloid- $\beta$ -related processes, *Biosensors* 10 (2020) 192.
- [38] S. Hameed, Z. Dai, Near-infrared fluorescence probes for surgical navigation, *Mater. Today Chem.* 10 (2018) 90–103.
- [39] R. Mallesh, J. Khan, P.K. Gharai, S. Ghosh, S. Garg, M.U. Arshi, S. Ghosh, High-affinity fluorescent probes for the detection of soluble and insoluble A $\beta$  deposits in alzheimer's disease, *ACS Chem. Neurosci.* 14 (2023) 1459–1473.
- [40] W. Ren, M. Xu, S.H. Liang, H. Xiang, L. Tang, M. Zhang, D. Ding, X. Li, H. Zhang, Y. Hu, Discovery of a novel fluorescent probe for the sensitive detection of  $\beta$ -amyloid deposits, *Biosens. Bioelectron.* 75 (2016) 136–141.
- [41] N.W. Smith, A. Alonso, C.M. Brown, S.V. Dzzyuba, Triazole-containing BODIPY dyes as novel fluorescent probes for soluble oligomers of amyloid A $\beta$ 1–42 peptide, *Biochem. Biophys. Res. Commun.* 391 (2010) 1455–1458.
- [42] L.P. Jameson, S.V. Dzzyuba, Aza-BODIPY: improved synthesis and interaction with soluble A $\beta$ 1–42 oligomers, *Bioorg. Med. Chem. Lett* 23 (2013) 1732–1735.
- [43] J. Killoran, L. Allen, J.F. Gallagher, W.M. Gallagher, F.O. Donal, Synthesis of BF $_2$  chelates of tetraarylazadipyrromethenes and evidence for their photodynamic therapeutic behaviour, *Chem. Commun.* 17 (2002) 1862–1863.
- [44] C.L. Teoh, D. Su, S. Sahu, S.W. Yun, E. Drummond, F. Prelli, S. Lim, S. Cho, S. Ham, T. Wisniewski, Y.T. Chang, Chemical fluorescent probe for detection of A $\beta$  oligomers, *J. Am. Chem. Soc.* 137 (2015) 13503–13509.
- [45] L. Quan, I. Moreno-Gonzalez, Z. Xie, N. Gamez, L. Vegas-Gomez, Q. Song, J. Gu, W. Lin, R. Gomez-Gutierrez, T. Wu, A near-infrared probe for detecting and interposing amyloid beta oligomerization in early Alzheimer's disease, *Alzheimer's Dementia* 19 (2023) 456–466.
- [46] T. Akasaka, H. Watanabe, M. Ono, *In vivo* near-infrared fluorescence imaging selective for soluble amyloid  $\beta$  aggregates using y-shaped BODIPY derivative, *J. Med. Chem.* 66 (2023) 14029–14046.
- [47] Y. Li, C. Tian, T. Xie, Q.L. Zhang, J. Liu, X.X. Yan, J. Dai, Y. Liang, M. Cui, Hydroxyethyl-modified cycloheptatriene-BODIPY derivatives as specific tau imaging probes, *ACS Med. Chem. Lett.* 14 (2023) 1108–1112.
- [48] M. Máximo-Canadas, I. Borges Jr., Absorption spectra of p-nitroaniline derivatives: charge transfer effects and the role of substituents, *J. Mol. Model.* 30 (2024) 120.
- [49] J.H. Xie, Z.Y. Xu, C.C. Deng, N.B. Li, H.Q. Luo, Rational design of push-pull fluorescent probe with extraordinary polarity sensitivity for VOCs chemical sensing and trace water detection, *Sensor. Actuator. B Chem.* 393 (2023) 134089.
- [50] C. Yan, Z. Guo, W. Chi, W. Fu, S.A. Abedi, X. Liu, H. Tian, W.H. Zhu, Fluorescence upmolung enables light-up sensing of N-acetyltransferases and nerve agents, *Nat. Commun.* 12 (2021) 3869.
- [51] C.J. Wu, X.Y. Li, T. Zhu, M. Zhao, Z. Song, S. Li, G.G. Shan, G. Niu, Exploiting the twisted intramolecular charge transfer effect to construct a wash-free solvatochromic fluorescent lipid droplet probe for fatty liver disease diagnosis, *Anal. Chem.* 94 (2022) 3881–3887.
- [52] C. Wang, W. Chi, Q. Qiao, D. Tan, Z. Xu, X. Liu, Twisted intramolecular charge transfer (TICT) from twists beyond TICT: from mechanisms to rational designs of bright and sensitive fluorophores, *Chem. Soc. Rev.* 50 (2021) 12656–12678.
- [53] K. Gade Malmos, L.M. Blancas-Mejia, B. Weber, J. Buchner, M. Ramirez-Alvarado, H. Naiki, D. Otzen, ThT 101: a primer on the use of thioflavin T to investigate amyloid formation, *Amyloid* 24 (2017) 1–6.
- [54] Y. Cheng, B. Zhu, Y. Deng, Z. Zhang, In vivo detection of cerebral amyloid fibrils with smart dicyanomethylene-4H-pyran-based fluorescence probe, *Anal. Chem.* 87 (2015) 4781–4787.
- [55] D. Escudero, Revising intramolecular photoinduced electron transfer (PET) from first-principles, *Acc. Chem. Res.* 49 (2016) 1816–1824.
- [56] E.E. Nesterov, J. Skoch, B.T. Hyman, W.E. Klunk, B.J. Bacskai, T.M. Swager, In vivo optical imaging of amyloid aggregates in brain: design of fluorescent markers, *Angew. Chem., Int. Ed.* 44 (2005) 5452–5456.
- [57] V.S. Kolmogorov, A.S. Erofeev, E.P. Barykin, R.V. Timoshenko, E.V. Lopatkina, S.A. Kozin, L.R. Gorbacheva, S.V. Salikhov, N.L. Klyachko, V.A. Mitkevich, C. R. Edwards, Scanning ion-conductance microscopy for studying  $\beta$ -amyloid aggregate formation on living cell surfaces, *Anal. Chem.* 95 (2023) 15943–15949.
- [58] W. Wu, L. Zhao, Y. Zhang, J. Wei, J. Han, Y. Zhang, Z. Zhao, Golgi-targeting viscosity probe for the diagnosis of Alzheimer's disease, *Sci. Rep.* 14 (2024) 1336.
- [59] J.L. Tomic, A. Pensalfini, E. Head, C.G. Glabe, Soluble fibrillar oligomer levels are elevated in Alzheimer's disease brain and correlate with cognitive dysfunction, *Neurobiol. Dis.* 35 (2009) 352–358.
- [60] H.S. Actor-Engel, S.L. Schwartz, K.C. Crosby, B.L. Sinnen, O. Prikhodko, H. J. Ramsay, J.N. Bourne, C.S. Winborn, A. Lucas, K.R. Smith, M.L. Dell'Acqua, Precision Mapping of amyloid- $\beta$  binding reveals perisynaptic localization and spatially restricted plasticity deficits, *Eneuro* 8 (2021).
- [61] Y.R. Huang, R.T. Liu, The toxicity and polymorphism of  $\beta$ -amyloid oligomers, *Int. J. Mol. Sci.* 21 (2020) 4477.
- [62] A.G. Kreutzer, G. Guaglianone, S. Yoo, C.M. Parrocha, S.M. Ruttenberg, R. J. Malonis, K. Tong, Y.F. Lin, J.T. Nguyen, W.J. Howitz, M.N. Diab, Probing differences among A $\beta$  oligomers with two triangular trimers derived from A $\beta$ , *Proc. Natl. Acad. Sci. USA* 120 (2023) e2219216120.
- [63] L. Xie, Y. Lai, F. Lei, S. Liu, R. Liu, T. Wang, Exploring the association between interleukin-1 $\beta$  and its interacting proteins in Alzheimer's disease, *Mol. Med. Rep.* 11 (2015) 3219–3228.

- [64] S.W. Yun, N.Y. Kang, S.J. Park, H.H. Ha, Y.K. Kim, J.S. Lee, Y.T. Chang, Diversity oriented fluorescence library approach (DOFLA) for live cell imaging probe development, *Acc. Chem. Res.* 47 (2014) 1277–1286.
- [65] L. Quan, J. Gu, W. Lin, Y. Wei, Y. Lin, L. Liu, H. Ding, C. Pan, Z. Xie, T. Wu, A BODIPY biosensor to detect and drive self-assembly of diphenylalanine, *Chem. Commun.* 55 (2019) 8564–8566.
- [66] F. Zeng, J. Yang, X. Li, K. Peng, C. Ran, Y. Xu, Y. Li, Versatile near-infrared fluorescent probe for in vivo detection of A $\beta$  oligomers, *Bioorg. Med. Chem.* 28 (2020) 115559.
- [67] D.P. Hanger, H.L. Byers, S. Wray, K.Y. Leung, M.J. Saxton, A. Seereeram, C. H. Reynolds, M.A. Ward, B.H. Anderton, Novel phosphorylation sites in tau from Alzheimer brain support a role for casein kinase 1 in disease pathogenesis, *J. Biol. Chem.* 282 (2007) 23645–23654.
- [68] S.J. Shah, Q. Zhang, J. Guo, H. Liu, H. Liu, J. Villà-Freixa, Identification of aggregation mechanism of acetylated PHF6\* and PHF6 tau peptides based on molecular dynamics simulations and markov state modeling, *ACS Chem. Neurosci.* 14 (2023) 3959–3971.
- [69] M. Gholampour, H. Seradj, A. Sakhteman, Structure–selectivity relationship prediction of tau imaging tracers using machine learning-assisted QSAR models and interaction fingerprint map, *ACS Chem. Neurosci.* 14 (2023) 1490–1502.
- [70] A. Ojida, M.A. Inoue, Y. Mito-Oka, I. Hamachi, Cross-linking strategy for molecular recognition and fluorescent sensing of a multi-phosphorylated peptide in aqueous solution, *J. Am. Chem. Soc.* 125 (2003) 10184–10185.
- [71] A. Ojida, M.A. Inoue, Y. Mito-Oka, H. Tsutsumi, K. Sada, I. Hamachi, Effective disruption of Phosphoprotein– protein surface interaction using Zn (II) dipicolylamine-based artificial receptors via two-point interaction, *J. Am. Chem. Soc.* 128 (2006) 2052–2058.
- [72] M. Ariza, H.C. Kolb, D. Moechars, F. Rombouts, J.I. Andrés, Tau positron emission tomography (PET) imaging: past, present, and future, *J. Med. Chem.* 58 (2015) 4365–4382.
- [73] M. Maruyama, H. Shimada, T. Suhara, H. Shinotoh, B. Ji, J. Maeda, M.R. Zhang, J. Q. Trojanowski, V.M. Lee, M. Ono, K. Masamoto, Imaging of tau pathology in a tauopathy mouse model and in Alzheimer patients compared to normal controls, *Neuron* 79 (2013) 1094–1108.
- [74] S. Baker, J. Götz, A local insult of okadaic acid in wild-type mice induces tau phosphorylation and protein aggregation in anatomically distinct brain regions, *Acta Neuro Comm* 4 (2016) 1–3.
- [75] A. Yagishita, T. Ueno, K. Tsuchihara, Y. Urano, Amino BODIPY-based blue fluorescent probes for aldehyde dehydrogenase 1-expressing cells, *Bioconjugate Chem.* 32 (2021) 234–238.
- [76] X.H. Xu, C. Liu, Y. Mei, Q.H. Song, BODIPY-based selenides as fluorescent probes for rapid, sensitive and mitochondria-specific detection of hypochlorous acid, *J. Mater. Chem. B* 7 (2019) 6861–6867.
- [77] J. Zhang, M. Yang, W. Mazi, K. Adhikari, M. Fang, F. Xie, L. Valenzano, A. Tiwari, F.T. Luo, H. Liu, Unusual fluorescent responses of morpholine-functionalized fluorescent probes to pH via manipulation of BODIPY's HOMO and LUMO energy orbitals for intracellular pH detection, *ACS Sens.* 1 (2016) 158–165.
- [78] I.V. Murray, M.E. Sindoni, P.H. Axelsen, Promotion of oxidative lipid membrane damage by amyloid  $\beta$  proteins, *Biochemist* 44 (2005) 12606–12613.